AFCRL-72-0154

SLANT RANGE VISIBILITY MEASUREMENT FOR AIRCRAFT LANDING OPERATIONS

By

WILLIAM VIEZEE
JOHN OBLANAS
RONALD T. H. COLLIS
Stanford Research Institute
Menlo Park, California 94025

CONTRACT NO. F19628-71-C-0152
Project No. 6670
Task No. 667004
Work Unit No. 66700401

FINAL REPORT

Period Covered: 1 April 1971 through 30 April 1972

February 1972

Contract Monitor: Eugene Y. Moroz
Meteorology Laboratory

Supported by

Department of Transportation
Transportation Systems Center
TSC No. DOT TSC-318
Cambridge, Massachusetts 02142

Prepared for

AIR FORCE CAMBRIDGE RESEARCH LABORATORIES
AIR FORCE SYSTEMS COMMAND
UNITED STATES AIR FORCE
BEDFORD, MASSACHUSETTS 01730

UNCLASSIFIED
Security Classification

DOCUMENT CONTROL DATA - R & D

(Security classification of title, body of abstract and indexing annotation must be entered when the overall report is classified)

1. ORIGINATING ACTIVITY (Corporate author)	2a. REPORT SECURITY CLASSIFICATION
Stanford Research Institute Menlo Park, California 94025	UNCLASSIFIED
	2b. GROUP

3. REPORT TITLE

SLANT RANGE VISIBILITY MEASUREMENT FOR AIRCRAFT LANDING OPERATIONS

4. DESCRIPTIVE NOTES (Type of report and inclusive dates)
Scientific. Final. 1 April 1971 - 30 April 1972

Approved
5 April 1972

5. AUTHOR(S) (First name, middle initial, last name)

William Viezee
John Oblanas
Ronald T. H. Collis

6. REPORT DATE	7a. TOTAL NO. OF PAGES	7b. NO. OF REFS
February 1972	100	4

8a. CONTRACT OR GRANT NO.	9a. ORIGINATOR'S REPORT NUMBER(S)
TSC No. DOT TSC-318 F19628-71-C-0152	SRI Project 1148
b. PROJECT NO. 6670-04-01	
c. DOD ELEMENT 62101F	9b. OTHER REPORT NO(S) (Any other numbers that may be assigned this report)
d. DOD SUPPLEMENT 686670	AFCRL-72-0154

10. DISTRIBUTION STATEMENT

A - Approved for public release; distribution unlimited.

11. SUPPLEMENTARY NOTES	12. SPONSORING MILITARY ACTIVITY
Supported by Department of Transportation, Transportation Systems Center 55 Broadway, Cambridge, Massachusetts 02142	Air Force Cambridge Research Laboratories (LY) L. G. Hanscom Field Bedford, Massachusetts 01730

13. ABSTRACT

A method of determining "slant visibility" by lidar observations from the ground during various degrees of fog and low cloud conditions has been investigated in an experimental program at a coastal site. The emphasis of the study was on the operational aspects of landing aircraft in Categories I and II conditions, and the first concern was to ascertain whether a pilot might be expected to obtain visual reference from the critical heights of 200 ft and 100 ft respectively. This depends primarily upon the transmittance along the slant paths from the cockpit to the ground. The aim of the lidar observations has thus been to determine the conditions of atmospheric transmittance aloft, with special reference to whether the appropriate minimum values are exceeded. Methods of analyzing the lidar returns from the atmosphere have been developed to derive information on the slant-path transmittance to a good accuracy when conditions are relatively homogeneous and when the visibility is very patchy as in low cloud and fog.

Lidar observations were made in a manner to simulate the operational geometry of slant visibility experienced by the pilot of a landing aircraft. For example, data on atmospheric backscatter versus range were obtained by pointing the lidar beam upward at a 15° elevation angle, thereby approximating the cockpit cutoff angle. Targets (wire-mesh and solid reflectors), mounted on top of towers, were aligned and spaced so as to intercept the 15° elevated lidar beam at heights of 200 ft and 100 ft, corresponding to the decision heights for the low-visibility landing Categories I and II, respectively. After a lidar pulse was transmitted through the array of elevated targets in order to record the target-reflected signals, a small change in the azimuth of the lidar was made to record a single-ended profile of atmospheric backscatter versus range along the 15° slant path immediately adjacent to the elevated targets. In this way, it was possible to compare determinations of transmittance derived from lidar observations of the atmosphere itself with path attenuation derived from measurements of the lidar signals from the reflecting targets.

Observations carried out in a variety of fog and low-ceiling conditions showed the great variability in transmittance over elevated paths that characterizes such conditions. With the lidar in a spatially fixed configuration pointing along the 15° elevated slant-path, 30 to 60 minute series of single-transmission measurements provided an adequate base for describing the prevailing slant visibility.

Within the limits of instrumental uncertainty, however, atmospheric extinction coefficients computed from single-ended observations made along the 15° elevated path show good comparison with the extinction coefficients derived from the measured transmittance between the targets. Values of slant visual range, derived from such single-ended observations, correspond well with the visual observations of the elevated targets made from the location of the lidar. It is concluded that the approach could lead to operationally useful measurements of "slant visibility" provided that the objective analysis techniques can be applied automatically in the most appropriate manner.

DD FORM 1 NOV 68 1473 (PAGE 1)

S/N 0101-807-6801

UNCLASSIFIED
Security Classification

14 KEY WORDS	LINK A		LINK B		LINK C	
	ROLE	WT	ROLE	WT	ROLE	WT
Slant visibility measurements by Lidar						
Slant visibility in fog and low clouds						
Lidar measurements of visibility						
Slant visibility for aircraft landing operations						
Operational application of lidar to aircraft landing operations						

AFCRL-72-0154

SLANT RANGE VISIBILITY MEASUREMENT FOR AIRCRAFT LANDING OPERATIONS

By

WILLIAM VIEZEE
JOHN OBLANAS
RONALD T. H. COLLIS
Stanford Research Institute
Menlo Park, California 94025

CONTRACT NO. F19628-71-C-0152
Project No. 6670
Task No. 667004
Work Unit No. 66700401

FINAL REPORT

Period Covered: 1 April 1971 through 30 April 1972

February 1972

Contract Monitor: Eugene Y. Moroz
Meteorology Laboratory

Approved for public release; distribution unlimited.

Supported by

Department of Transportation
Transportation Systems Center
TSC No. DOT TSC-313
Cambridge, Massachusetts 02142

Prepared for

AIR FORCE CAMBRIDGE RESEARCH LABORATORIES
AIR FORCE SYSTEMS COMMAND
UNITED STATES AIR FORCE
BEDFORD, MASSACHUSETTS 01730

ABSTRACT

A method of determining "slant visibility" by lidar observations from the ground during various degrees of fog and low cloud conditions has been investigated in an experimental program at a coastal site. The emphasis of the study was on the operational aspects of landing aircraft in Categories I and II conditions, and the first concern was to ascertain whether a pilot might be expected to obtain visual reference from the critical heights of 200 ft and 100 ft respectively. This depends primarily upon the transmittance along the slant paths from the cockpit to the ground. The aim of the lidar observations has thus been to determine the conditions of atmospheric transmittance aloft, with special reference to whether the appropriate minimum values are exceeded. Methods of analyzing the lidar returns from the atmosphere have been developed to derive information on the slant-path transmittance to a good accuracy when conditions are relatively homogeneous and when the visibility is very patchy as in low cloud and fog.

Lidar observations were made in a manner to simulate the operational geometry of slant visibility experienced by the pilot of a landing aircraft. For example, data on atmospheric backscatter versus range were obtained by pointing the lidar beam upward at a 15° elevation angle, thereby approximating the cockpit cutoff angle. Targets (wire-mesh and solid reflectors), mounted on top of towers, were aligned and spaced so as to intercept the 15° elevated lidar beam at heights of 200 ft and 100 ft, corresponding to the decision heights for the low-visibility landing Categories I and II, respectively. After a lidar pulse was transmitted through the array of elevated targets in order to record

the target-reflected signals, a small change in the azimuth of the lidar was made to record a single-ended profile of atmospheric backscatter versus range along the 15° slant path immediately adjacent to the elevated targets. In this way, it was possible to compare determinations of transmittance derived from lidar observations of the atmosphere itself with path attenuation derived from measurements of the lidar signals from the reflecting targets.

Observations carried out in a variety of fog and low-ceiling conditions showed the great variability in transmittance over elevated paths that characterizes such conditions. With the lidar in a spatially fixed configuration pointing along the 15° elevated slant-path, 30 to 60 minute series of single-transmission measurements provided an adequate base for describing the prevailing slant visibility.

Within the limits of instrumental uncertainty, atmospheric extinction coefficients computed from single-ended observations made along the 15° elevated path show good comparison with the extinction coefficients derived from the measured transmittance between the targets. Values of slant visual range, derived from such single-ended observations, correspond well with the visual observations of the elevated targets made from the location of the lidar. It is concluded that the approach could lead to operationally useful measurements of "slant visibility" provided that the objective analysis techniques used can be applied automatically in the most appropriate manner.

CONTENTS

CONTENTS (Continued)

ILLUSTRATIONS

ILLUSTRATIONS (Continued)

ILLUSTRATIONS (Continued)

ILLUSTRATIONS (Continued)

ILLUSTRATIONS (Concluded)

TABLES

ACKNOWLEDGMENTS

In addition to the authors, the SRI team included Mr. William Dyer, Senior Electromechanical Technician, and Mr. H. Shigeishi, Mathematician.

Thanks are due to Mr. Eugene Y. Moroz, AFCRL, for his help and interest throughout the project. We are very grateful for the help provided by personnel of the Pillar Point site, particularly Mr. Dennis Inch, Manager of the Western Test Range, and Col. Oliver C. Fought at Vandenberg AFB, who made the necessary arrangements for us to use the site. In addition, we acknowledge the generous assistance provided by Mr. Anthony Lazzara of STI, Inc.

I INTRODUCTION AND BACKGROUND

The possibility of measuring atmospheric visibility by lidar has generated much interest primarily because of the potential of using a single-ended laser device in aircraft landing operations to measure slant visibility, a quantity that has been most elusive to routine observation. Although many techniques have been suggested, only a few concepts have been tested in the real atmosphere under critical low-visibility conditions of fog (e.g., Brown, 1967).*

In January 1968, Stanford Research Institute activated a pulsed ruby lidar at Hamilton AFB, California, under conditions of low ceiling and visibility in order to explore the operational utility of the lidar in cloud ceiling and visibility determination (Viezee et al., 1969). Results demonstrated that the lidar could obtain detailed information on cloud conditions at locations along the approach path, where, because of the marshes and open water, conventional ceilometers could not be operated. The possibility of processing the lidar observations to obtain quantitative data on the atmospheric extinction coefficient--i.e., on the optical parameter significant to "visibility" determination--was also explored, with indications that operationally useful analyses were feasible.

The exploratory work initiated at Hamilton AFB was followed by a more comprehensive effort, made in the summer of 1970, to investigate the theoretical and practical aspects of determining atmospheric visibility by lidar (Collis et al., 1970). An experimental pulsed neodymium lidar system was modified and calibrated to obtain accurate data on atmospheric

---

* References are listed at the end of the report.

optical properties in the strongly scattering conditions of dense fog. To operate in such conditions, the system's dynamic range was extended to 50 dB by using a two-stage receiver system, in which the high-sensitivity element was operated in such a way as to avoid saturation from close-in signals. In addition, the transmitter and receiver beams were made coaxial to make possible close-range observations. Field trials were carried out during conditions of fog at Half Moon Bay, California, and at Arcata, California, in May/June and August 1970, respectively. At the Arcata site, observations were made in conjunction with measurements by an array of up to five conventional (AN/GMQ-10) transmissometers at the NBS test facility. A particular feature of the lidar observations was the use of passive reflectors or targets set out along the surface to provide information on atmospheric extinction. This was accomplished by comparing the intensity of lidar return signals from near and far targets, to provide a measure of attenuation averaged over the path between them. To make this possible, the near targets were in the form of wire-mesh screens and were thus semitransparent (transmissions of 75 and 65 percent). The farther targets were solid, diffuse reflectors. Atmospheric transmittances obtained from the lidar/target data showed high correlation (correlation coefficient 0.92) with data from the conventional transmissometers for comparable horizontal paths under a variety of visibility conditions. Single-ended lidar profiles of atmospheric backscatter versus range were obtained along horizontal paths adjacent to the passive targets and to a 500-ft base-line transmissometer. A total of 32 separate values of atmospheric transmittance were computed from these lidar data using the "slope" method. These values were compared with the transmittance measured by the transmissometer. The overall comparison was good and supported the hope of obtaining objective measurements of slant visibility conditions in fog and low cloud remotely by lidar observations.

This report extends the previous work and presents lidar observations of slant-path visibility made under various conditions of low clouds and fog at the coastal site of Pillar Point, California, in the summer and early fall of 1971. The objective of the experiment was to investigate, analyze, and verify the lidar technique of measuring runway slant-range visibility.

II SUMMARY AND CONCLUSIONS

In pursuing the contract objective, emphasis was placed on the operational aspects of landing aircraft in Categories I and II conditions, and the first concern was to ascertain whether or not, on the basis of lidar measurements, a pilot might be expected to obtain visual reference from the critical heights of 200 ft and 100 ft, respectively. Lidar observations were made in a manner to approxima . closely the operational geometry of slant visibility experienced by the pilot of a landing aircraft. For example, data on atmospheric backscatter versus range were obtained by pointing the lidar beam upward at a 15° elevation angle, thereby approximating the cockpit cutoff angle. Targets (wire-mesh and solid reflectors), mounted on top of towers, were aligned and spaced so as to intercept the 15° elevated lidar beam at heights of 200 ft and 100 ft, corresponding to the decision heights for the low-visibility landing Categories I and II, respectively. Lidar observations of slant visibility were obtained from single-pulse transmissions, made at intervals of approximately 1 minute. With these experimental conditions and also with the physical conditions encountered, an observation period of 30 to 60 minutes was needed fully to characterize a prevailing fog condition. Data were collected during daytime hours because of a heavy reliance on visual observations for guidance and verification of the lidar/slant-visibility experiment. The lidar equipment that was needed to make the required series of slant-path observations under the various fog conditions is discussed in Section III. Details on the techniques of observation and data analysis are given in Section IV. Results of the observational program are presented in Sections V and VI.

On the 1- to 2-minute time scale used in the observational program, the lidar data show large temporal fluctuations in the slant-range atmospheric extinction coefficient. These fluctuations, which are characteristic of the coastal fog conditions encountered at Pillar Point, render a single measurement of slant visibility operationally useless.

With the lidar in a spatially fixed configuration, pointing along the 15° elevated slant path, realistic information on the slant-visibility conditions that prevailed during the occurrence of low clouds and fog is derived from 30- to 60-minute series of single-transmission measurements. Within the limits of instrumental uncertainty, the atmospheric extinction coefficients computed from single-ended data obtained along the fixed 15° slant path show good comparison with those obtained along a comparable path from the elevated-target data. Values of slant visual range obtained from the single-ended data using Koschmieder's law are in good agreement with visual observations of the elevated targets made from the location of the lidar. A contrast threshold of 0.02 gives superior results to the more conservative value of 0.055.

When the lidar is operated in a scanning configuration, both the time and space variabilities enter into the data, thus introducing additional complexity to the data analysis and interpretation.

The lidar equipment and the data analysis technique used in the study are considered a research tool rather than a system that can be readily implemented in an automated, operational device for routine measurements of slant visibility. Although results appear to be realistic, the true validity, accuracy, and operational feasibility of the technique as applied to the aircraft landing problem remain to be verified.

III EQUIPMENT AND INSTRUMENTATION

The lidar equipment and auxiliary instrumentation used in the lidar/slant-visibility project were basically the same as that described previously (Collis et al., 1970). Accordingly, a detailed description will not be repeated here. Only the significant differences in the equipment used will be discussed. The basic characteristics of the lidar system are listed in Table 1.

Table 1

SRI MARK V LIDAR CHARACTERISTICS

Transmitter	
Laser Material	Neodymium Glass
Wavelength	10,600 Å
Spectral Line Width	90 Å
Q-Switch	Rotating Prism
Collimating Optics	Refractive, 2-inch diameter
Beamwidth	0.4 Milliradian
Peak Power Output	50 Megawatts
Pulse Length	20 Nanoseconds
Pulse Repetition Rate	12 per minute
Receiver	
Optics	6-inch f/4 Newtonian Reflector
Field of View	1 Milliradian
Predetection Filter Wavelength Interval	100Å
Detectors (Two)	RCA 7102 Photomultiplier (S-1 Response)
Postdetection Bandwidth	10 MHz
Receiver	Logarithmic

A. Receiver and Transmitter Calibration

In order to reduce some residual inaccuracies inherent in the dual receiver transfer functions, the calibration methods and lidar operating techniques were upgraded, with considerable emphasis on accuracy, stability, and repeatability of the lidar data. Because extensive modification of the existing equipment was beyond the scope of the current work, the effort was concentrated on reducing to an absolute minimum any remaining effects that would cause variability in the lidar data. Several specific examples of this effort are outlined below:

(1) Because variations in the amplitude of the 260-volt gating pulse applied to the first dynode of the gated photomultiplier have considerable influence on the photomultiplier gain, a digital voltmeter was added to monitor continuously the gating pulse amplitude.

(2) The interaction of the photomultiplier operating voltage and gating pulse amplitude was investigated and refined to produce optimum gain of the first dynode stage of the photomultiplier.

(3) The calibration instrumentation was modified to eliminate the effect of power supply ripple on the accuracy of the receiver calibration.

(4) Receiver transfer function calibrations were performed a number of times both in the laboratory and in the field. The resulting data were analyzed to assess short-term and long-term repeatability of the lidar measurements.

(5) During the data collection phase, extensive use was made of neutral density filters on both detectors to eliminate any problems related to detector saturation.

The net result of the effort was to minimize errors in lidar data associated with the calibration procedures. Further improvements in data accuracy can be accomplished by improvements in the optical calibration equipment.

B. Dual Detectors

The concept of a receiver with dual detectors was originally intended to accommodate a receiver dynamic range twice as great as that of one detector alone. This could be accomplished by separately recording the data from the high-sensitivity and low-sensitivity detectors and combining these two pieces of information during data processing. However, the dual detectors were not used as originally planned because correlation of the data recorded simultaneously by the two detectors revealed inconsistencies in the bandwidth characteristics of the logarithmic amplifiers. Fortunately, it was found that the dynamic range of the return signals received during dense fog was lower than anticipated and could, therefore, be recorded by one detector. During large changes in fog density, neutral density filters were used to keep the lidar signals within the dynamic range of a single detector. The dual detector arrangement within the lidar receiver found its greatest use in evaluating the logarithmic amplifiers.

C. Logarithmic Amplifiers

The lidar target data on slant visibility collected and analyzed during July and the beginning of August 1971 revealed certain inconsistencies in the data recorded simultaneously by the two detectors. The inconsistencies produced differences in the atmospheric extinction coefficients obtained from the two sets of data. The differences in the recorded data were found to be caused by individual differences in the electrical characteristics of the two logarithmic amplifiers. Specifically, variations in the instantaneous bandwidth of the two amplifiers as a function of input signal amplitude were detected.

The two log amplifiers used previously at Arcata, California (Collis et al., 1970), and at the beginning of this project (hereinafter referred to as loggers 1 and 2) were designed and constructed at SRI several years

ago. At that time, log amplifiers of the required characteristics were not commercially available. In the SRI design the bandwidth of the amplifier is a direct function of the input signal amplitude (as in all previous designs of wide-bandwidth log video amplifiers), and the nonlinear function is accomplished by a forward-biased semiconductor diode. Over a selected operating range, the voltage across the junction of the diode is approximately proportional to the logarithm of the current through this diode. The bandwidth of the log amplifier is determined by the instantaneous impedance (time-varying) of the log diode and the shunt capacitance across the diode (which is fixed) acting as a simple RC filter. The diode impedance, in turn, is an inverse function of the diode current. Thus, at high input currents (corresponding to high signal levels), the low impedance of the diode in parallel with the stray capacitance across the diode results in a high-frequency cutoff of approximately 10 MHz. At low signal levels, the high impedance of the diode is paralleled with the same value of stray capacitance, resulting in a high-frequency cutoff as low as 200 kHz. In all cases, the high-frequency roll-off with increasing frequency is 20 dBV/decade characteristic of a simple RC filter.

The amplitude-bandwidth characteristics of log amplifiers described above is well known; however, the impact of this characteristic upon the quality of lidar data is critically dependent upon the specific lidar application under consideration, and must be evaluated experimentally, the major criterion being the required accuracy of the data.

Midway through the observational program, a log amplifier of new design (hereinafter referred to as logger 3) became available for the first time.* A prototype model of logger 3 was obtained and evaluated first in

---

* Logger 3 is a proprietary development of Scientific Technology, Inc. (STI), 1157 San Antonio Rd., Mountain View, Califorhia 94040.

the laboratory and later under experimental conditions at Pillar Point. The characteristics were not precisely suited for the application to fog monitoring, but the differences were relatively minor and did not affect the resulting evaluation. For example, the output scale factor of the prototype was 100 mV/dB input compared to our usual value of 20 mV/dB input.

The significant difference between logger 3 and loggers 1 and 2 is that the bandwidth is independent of input signal amplitude. This characteristic allows more accurate measurement of path attenuation from the reflecting-target returns, and also results in improved estimates of atmospheric extinction from single-ended lidar traces.

A comparison of the data output from logger 1 and logger 3 is presented in Figure 1. The two lidar traces of Figure 1(a) are 15° elevated-target returns recorded simultaneously by the two detectors from one transmitted lidar pulse under clear conditions. The upper trace was obtained from logger 1 and the lower trace from logger 3. Comparison of the two traces shows the absence of the exponential decay ("tail") at the base of the three target returns in the lower trace.

Single-ended lidar traces taken under low-visibility conditions are illustrated in Figure 1(b). The difference in slope of the two data samples at the low-voltage output at ranges ≥0.09 km is noteworthy.

The performance of the prototype logger 3 was investigated in detail within the limitations of the existing SRI calibration instrumentation and technique. The main objective of the laboratory calibration was to determine whether the bandwidth was sufficient to provide high-resolution lidar data, to verify the linearity and accuracy of the logarithmic function, to determine whether the log amplifier bandwidth was truly independent of the signal amplitude.

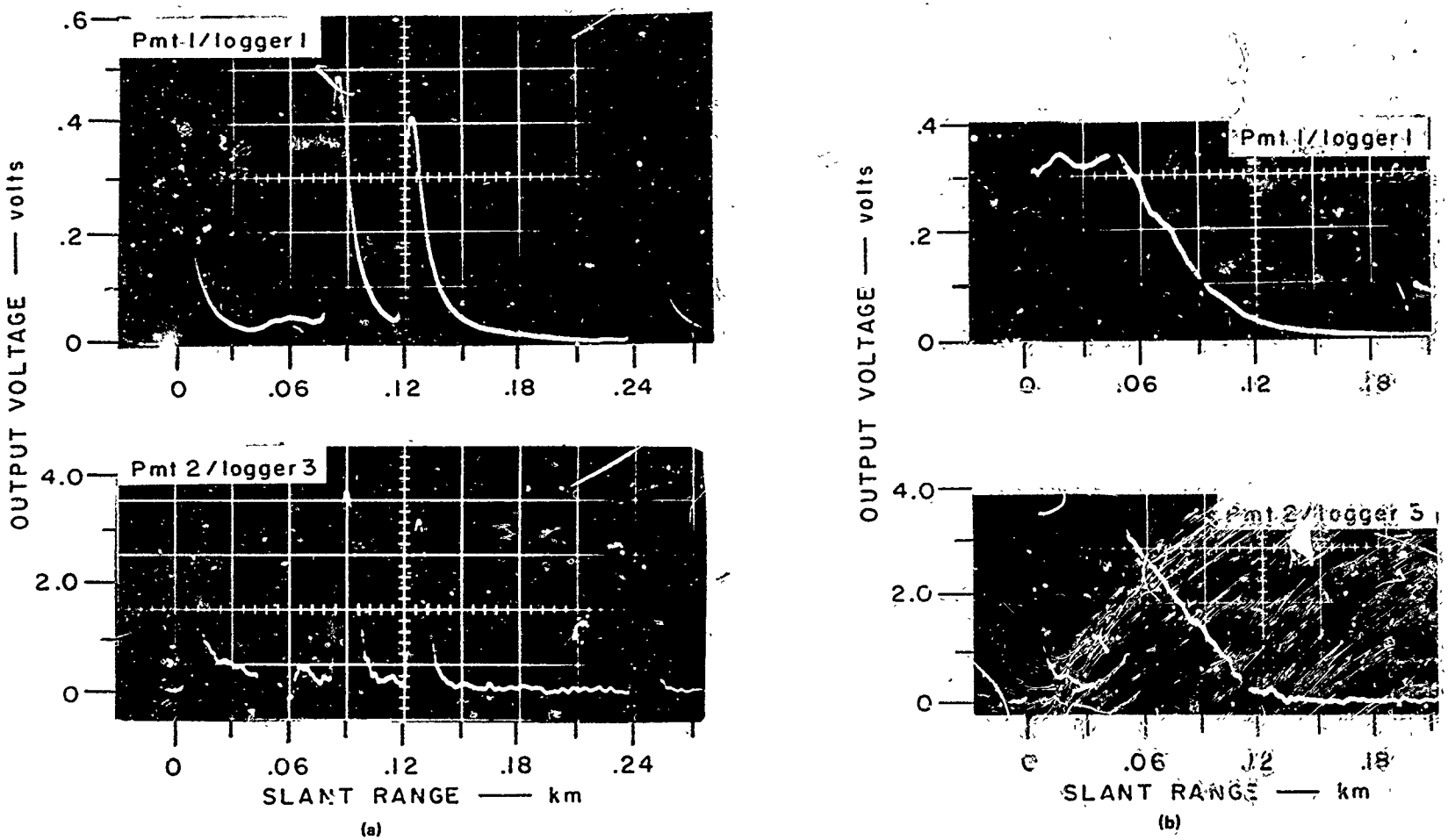

FIGURE 1 PHOTOGRAPHS OF OSCILLOSCOPE DISPLAYS SHOWING (a) SIGNALS RECEIVED FROM ELEVATED TARGETS AND (b) SLANT-PATH TRACES OF ATMOSPHERIC BACKSCATTER SIGNAL VERSUS RANGE RECORDED SIMULTANEOUSLY BY TWO PHOTOMULTIPLIERS CONNECTED TO LOGARITHMIC AMPLIFIERS OF DIFFERENT DESIGN

The initial results of the laboratory investigation were promising although improvements in calibration equipment and calibration techniques are required to use the capabilities of the new amplifier fully.

Once the general characteristics of logger 3 were determined in the laboratory, the amplifier was installed in the Mk V lidar system located at Pillar Point on 17 August 1971, and final calibration of the receiver transfer function was performed there. Experimental data were taken under both clear and foggy conditions using both logger 1 and logger 3. The logger 1 was connected to the upper (low-sensitivity) detector (pmt 1), and the new logger 3 was connected to the lower (high-sensitivity) detector (pmt 2). Neutral density filters were introduced into the optical paths of both detectors to compensate for their differences in sensitivity so that comparable data were obtained from both channels of the receiver. The analysis and interpretation of simultaneous data obtained from the two receiver channels are presented in Section V.

D. A Practical, Operational Slant-visibility Measuring System

The Mk V neodymium lidar used in this study was satisfactory for research purposes but cannot in its present configuration be expected to serve as a practical, operational system. Also, the methods of recording and processing the data, and of extracting information on slant-range visibility, were specifically designed for the research task at hand, and not for an operational system. However, as a direct result of the research carried out under this and the previous program (Collis et al., 1970), an initial evaluation of the technical feasibility of an operational system, along with several concepts of how such a system might be realized, can be made. For purposes of discussion, the practical, operational system is divided into two major components: (1) the optical sensor (lidar) and (2) the associated data recording, processing, transmission, and display system.

1. The Optical Sensor

The potential eye-safety hazard generally associated with Q-switched ruby or neodymium lasers restricts their use in any operational application to slant-range visibility monitoring. The American National Standards Institute (through its Z-136 committee) is currently formulating a laser safety standard that will have the support of the armed services as well as other government agencies and private industry. The safety standard is expected to be published during 1972 and when accepted will much more clearly define the eye-damage hazard.

When monitoring runway slant-range visibility in its configuration used in this research study, the lidar sensor would be located along the runway near the approach lights, with a fixed beam at approximately 15°-18° elevation angle. This beam geometry will monitor the visibility conditions along the pilot's line of sight as he looks from the cockpit at the approach lights from an altitude of approximately 200 ft. When the lidar beam is fixed and does not scan in either azimuth or elevation, the eye-safety hazard exists only at the instant when an aircraft, on its final approach, passes through the 200-ft decision height. Although the eye-safety hazard could be minimized by simply disabling the lidar sensor during the time that a landing aircraft passes the 200-ft decision height, this solution is not satisfactory since other aircraft flying at higher altitudes could intercept the transmitted beam.

Two alternatives to minimize (or possibly eliminate) the potential eye-damage hazard appear possible. The first is to select laser wavelengths that are not transmitted by the ocular fluids within the human eye. The eye-damage effects are then confined to the cornea and ocular fluids, and not the sensitive retina of the eye. The net result is that the damage threshold would be increased substantially over lasers operating in the visible region of the spectrum. Lasers that fall in this category include

erbium (1.54 μ), holmium (approximately 2.1 μ), carbon monoxide (approximately 5 μ), and the carbon dioxide "TEA" laser (10.6 μ). If high pulse-repretition rates can be achieved with the above lasers, then the possibility of signal averaging to increase the overall sensitivity may overcome in part the lack of detector sensitivity at these wavelengths.

When working at wavelengths significantly different from the visible, the question arises as to how representative the atmospheric extinction measurements made at an infrared wavelength are of the atmospheric extinction that is related to the human eye response. The present lack of suitable detectors capable of operating at ambient temperatures may be somewhat of a drawback to operational sensor systems using infrared lasers.

A second alternative that may minimize the eye-damage hazard is to operate at considerably lower peak powers but at high repetition rates. Signal integrating techniques can be used to improve the overall sensitivity, and this approach could be beneficial in averaging out small-scale fluctuations in the scattering characteristics of the atmosphere.

Because of the present uncertainties in eye safety, a detailed design of lidar sensors for slant-visibility measurements is considered premature at this time. Many of the alternative infrared laser sources are still in early developmental stages, and a detailed description of conceptual IR lidar systems would be rapidly obsolete.

2. The Data-processing System

Although the analysis and interpretation techniques described in this report can produce good results if applied in optimum fashion, depending upon the degree of homogeneity of conditions along the path of observation, such application requires the intervention of human intelligence, even though objective and computerized methods were used to make the necessary calculations. For an ultimate, operationally useful system,

the analysis technique must be made fully automatic. This poses problems since distinctions that can be readily made with the aid of human judgment are cumbersome to accomplish by automatic techniques--particularly when the possibility of error is highly undesirable.

The analysis technique essentially involves two steps: firstly, the selection of the appropriate technique to apply to each segment of the slant path, and secondly, the derivation of the extinction coefficient by the chosen technique. For an operational system, further steps need to be taken to relate the instrumental observations of extinction coefficient or slant-path transmittance to "visibility" conditions in terms of the pilot's visual acuity, ambient lighting conditions, and the contrast of the ground reference (which, in most cases, would be the guidance lights of the approach zone).

Although it is possible to consider a completely "software" solution to the analysis and interpretation problem--in which each lidar observation is fully digitized and subjected to a complex computer analysis--such an approach is unattractive for many reasons. It would require fast analog-to-digital conversion of the lidar signals and the application of at least a dedicated minicomputer to derive solutions. Although the costs of such converters and computer facilities are declining steadily, the cost of such a system would still be considerable and the computational requirements would be complex and cumbersome. A short-cut might be provided by sampling at a series of range gates, using the integration of the returns from a number of pulses to develop measurable signals in each range-gate store. The relationship of such signals as a function of range could be fairly simply established by ratio techniques or, in digital form, coincidence circuitry. Where a series of signals over consecutive range increments exhibited a consistency within prescribed limits that indicated returns from a homogeneous atmosphere, the "slope" method could be used to derive the extinction coefficient for

the segment in question. For transitional segments, a simple logical program could determine major features, such as cloud-base height; alternatively, for areas in which cloud density is increasing or marked inhomogeneity is apparent, a purposely high extinction coefficient could be applied, with the object of at least providing a worst-case assessment of path "visibility."

Another approach would be to accomplish the required signal processing in real time using conventional wideband analog techniques under digital control and timing. This approach eliminates the need and expense of a fast analog-to-digital converter required in the purely digital approach. The output of the photomultiplier detector after passing through an accurately calibrated logarithmic amplifier is applied to a real-time analog processor that eliminates the inverse range-squared attenuation effects in the raw data. This could be accomplished by generating the function 2 log R and adding it to the lidar signal. The resulting signal would then be differentiated to obtain a voltage proportional to the slope of the input waveform. This voltage, which is related to the atmospheric extinction coefficient, could be digitized and transmitted to the display in recording electronics, or it could be accumulated in a register and averaged using conventional digital computational techniques.

The choice of appropriate data-processing techniques is obviously much dependent upon the nature of the data acquisition system used. The above discussion is intended only to draw attention to the nature of the problem, and the difficulties that would have to be overcome. The concepts discussed, however, are illustrative of the approaches open, and in the light of current progress in low-cost computational and data-processing devices, suitable solutions are likely to be attainable within reasonable constraints as to cost and complexity with appropriate research and development.

IV TECHNIQUES OF OBSERVATION AND DATA ANALYSIS

A. Observation Technique

Observations were made in a manner to simulate the operational geometry of slant visibility experienced by a landing aircraft. For example, data on atmospheric backscatter versus range were obtained by pointing the lidar beam upward at a 15° elevation angle, thereby approximating the cockpit cutoff angle. Targets (passive reflectors) mounted on temporary towers were aligned and spaced so as to intercept the 15° elevated lidar beam at heights of 200 ft and 100 ft, corresponding to the decision heights for the low-visibility landing Categories I and II, respectively. Figure 2 shows a schema of the experimental lidar/target geometry. Figure 3(a) shows a panoramic view of the experimental site; Figure 3(b) presents a close-up of the targets as they are aligned on top of the towers. Semitransparent wire-mesh targets are mounted at the top of Towers A (90 ft above the ground) and B (130 ft above the ground). A solid target* is mounted at the top of Tower C (240 ft above the ground). Targets T_B and T_C intercept the 15° elevated lidar beam at heights (above the horizontal plane) of 100 ft and 200 ft, respectively. Targets are also located at the 0° elevation angle of the towers to enable reference measurements related to horizontal visibility.

Lidar data were collected by alternatively firing the lidar at and slightly off the 15° elevated targets at intervals of 1 minute. After

---

* The solid target is constructed of plastic-coated plywood. The reflecting surface is composed of one coat of "White Velvet" enamel paint (Minnesota Mining and Manufacturing Co., Stock No. 108A10) over two coats of flat white primer (for further details on the construction of the passive reflectors, see Collis et al., 1970).

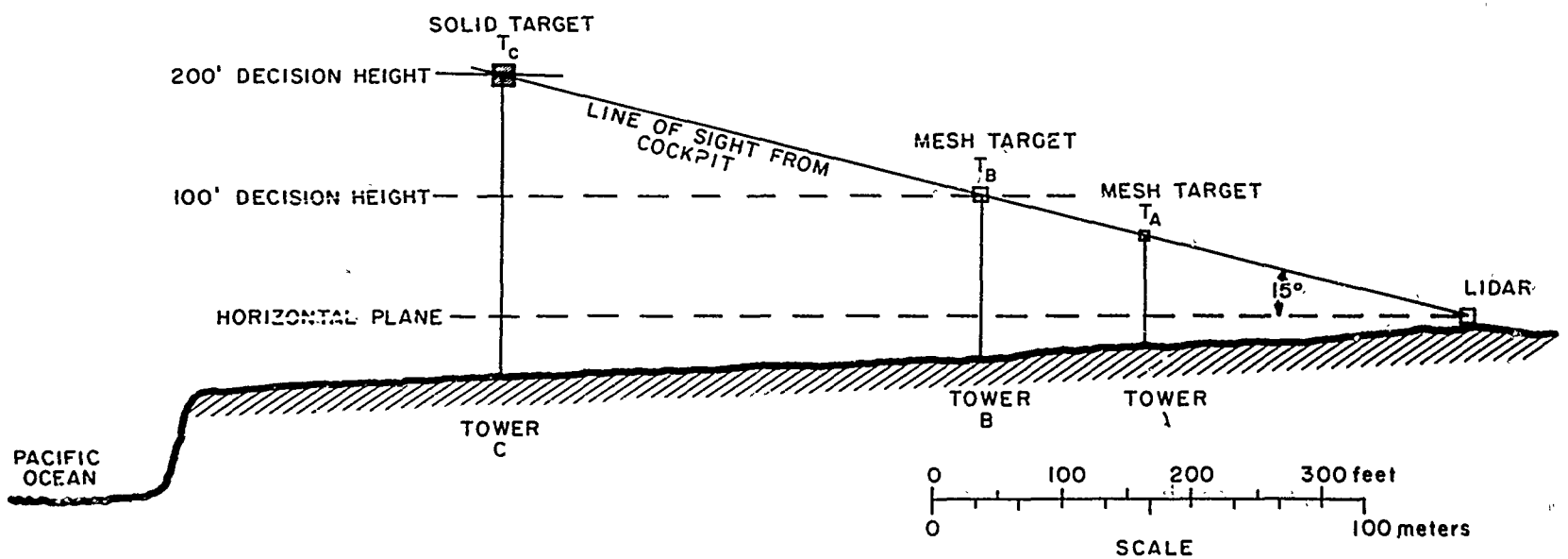

FIGURE 2 TARGET GEOMETRY OF LIDAR/SLANT VISIBILITY EXPERIMENT AT PILLAR POINT, CALIFORNIA

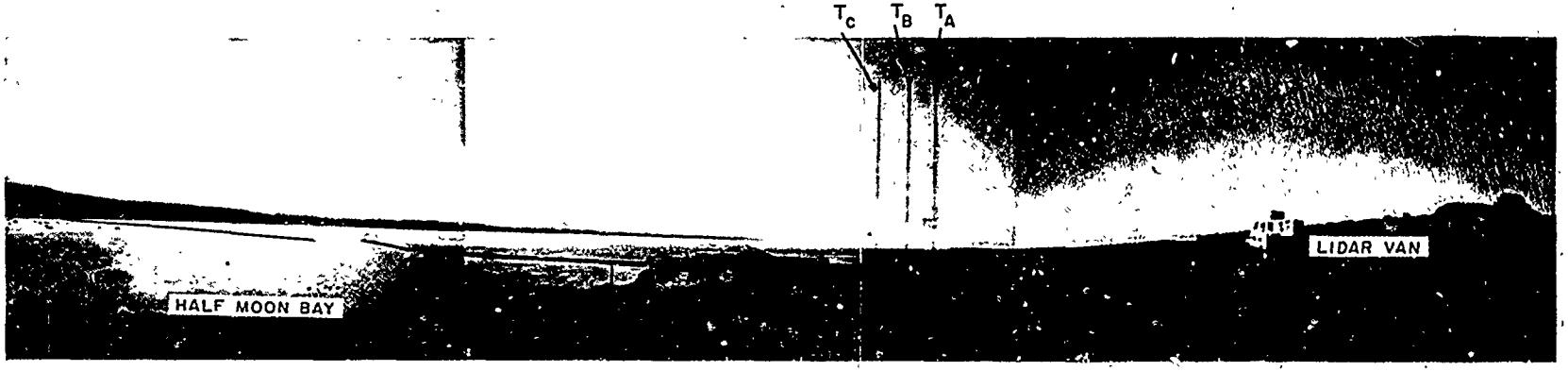

(a) VIEW OF EXPERIMENTAL SITE USED IN LIDAR/SLANT VISIBILITY OBSERVATION PROGRAM

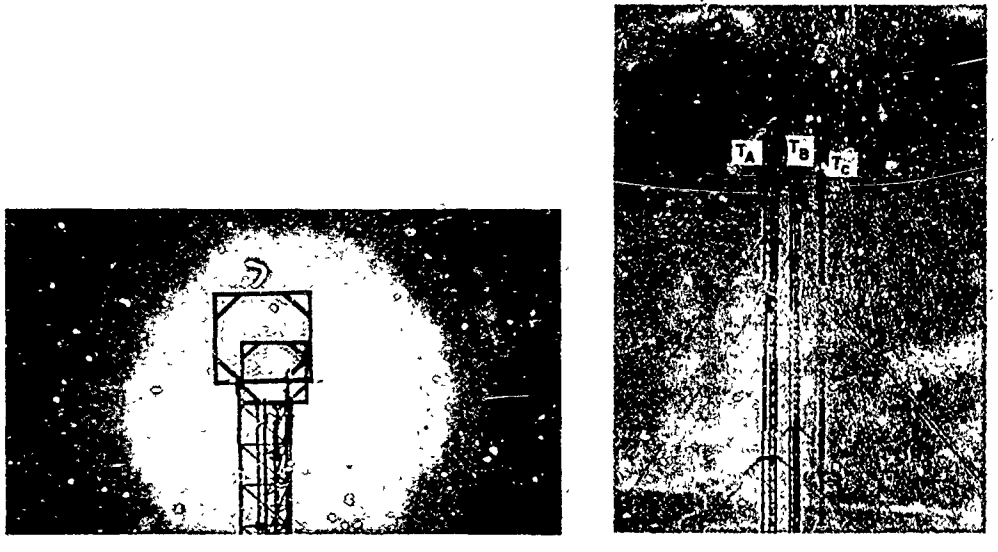

(b) VIEWS OF 15° ELEVATED-TARGET ARRANGEMENT

FIGURE 3 VIEWS OF EXPERIMENTAL SITE AND TARGETS

a lidar pulse was transmitted through the array of targets in order to record the target-reflected signals, a small change in the azimuth of the lidar was made to record a single-ended profile of atmospheric backscatter versus range along the 15° slant path immediately adjacent to the targets. By making observations in this way, one can compare determinations of extinction derived from lidar observations of the atmosphere itself with path attenuation derived from measurements of the lidar signals from the reflecting targets. A 1-minute time interval was needed to manually change the azimuth of the lidar and the neutral density filters in front of the photomultipliers (see Section III, on Instrumentation and Equipment). The data were recorded simultaneously from the two photomultipliers of the dual receiver system, and the 1-minute interval between single-pulse transmissions gave an adequate data base without redundancy. Samples of observations were also collected by scanning the lidar from 15° to 0° at intervals of 3° in elevation angle.

Because of a heavy reliance on visual observations for guidance and verification of the lidar/slant-visibility experiment, all data were collected during daytime hours.

B. Data Analysis Technique

The ratio of the target-reflected signals received from two successive targets is related to the atmospheric extinction coefficient averaged over the distance between the two targets (Collis et al., 1970). Thus, at each lidar-pulse transmission through the elevated target array, two values of atmospheric extinction are obtained, one averaged over the distance T_A to T_B (37 m) and the other averaged over the distance T_B to T_C (117 m). Figure 4 shows an example of target signals received from the semitransparent mesh targets (T_A and T_B) and from the solid target (T_C) during clear and foggy conditions.

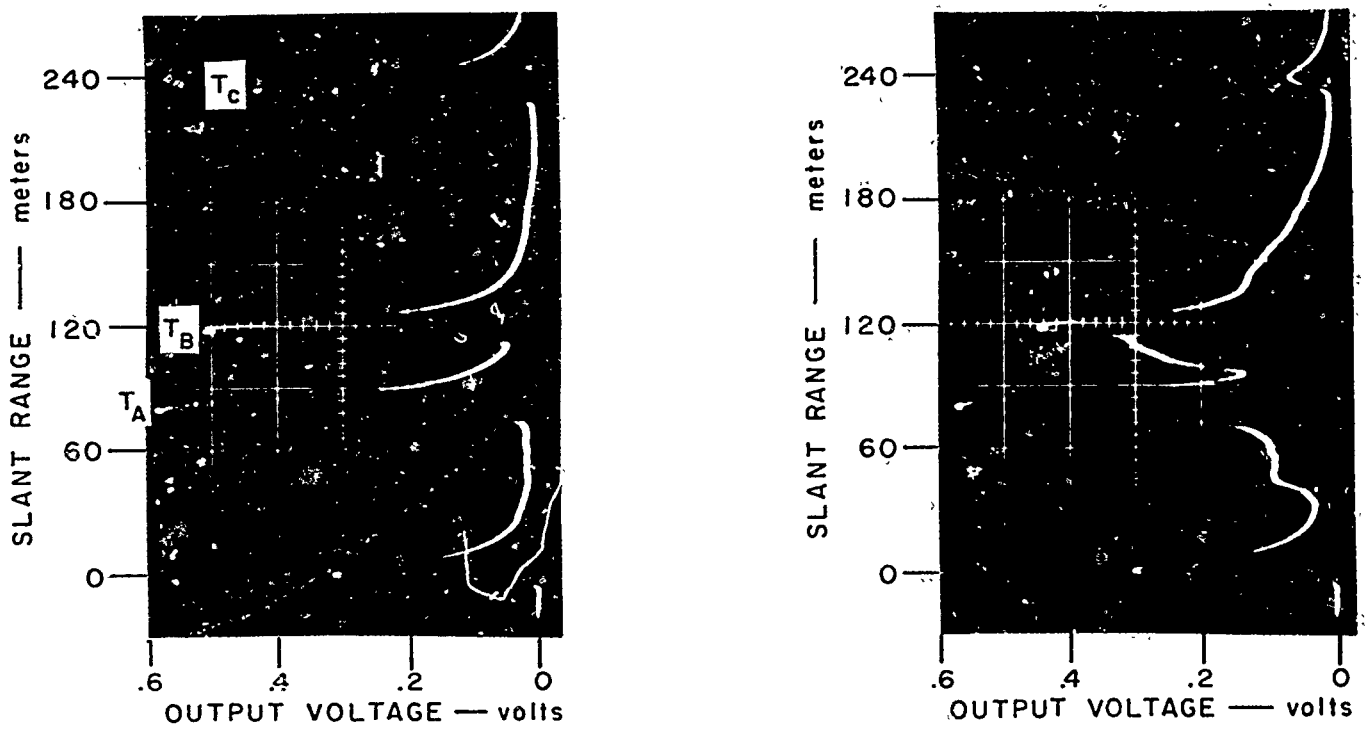

FIGURE 4 PHOTOGRAPHS OF OSCILLOSCOPE DISPLAY SHOWING LIDAR SIGNALS RECEIVED FROM THE 15° ELEVATED TARGETS DURING CONDITIONS OF (a) CLEAR AIR AND (b) FOG, AT PILLAR POINT, CALIFORNIA, ON 4 AUGUST 1971

The slant-path single-ended profiles of atmospheric backscatter versus range are analyzed using the "slope" method described in an earlier report (Collis et al, 1970). In summary, the single-ended lidar data are photographically recorded from the oscilloscope in terms of output voltage versus range and are digitized and then computer-processed in terms of the so-called S-function versus range R. In the digitization of each oscilloscope trace, the output voltage is put on tape as a function of range at intervals of approximately 1.5 meters. The tape provides the input to a computer program that corrects recorded lidar backscatter signals for the inverse range-squared $(1/R^2)$ attenuation and converts voltage output to relative decibel (dB) input by applying the calibration data of the photomultiplier/logarithmic-amplifier component of the receiver system. Thus, for the ith trace at the jth range, we have

$$S_{i,j} = 10\psi_c \{V_{i,j}\} + 20 \log_{10} R_j \quad ,$$

where

$V_{i,j} \equiv$ recorded voltage of ith trace at jth range R_j

$\psi_c \equiv$ an operator, determined from the system calibration, which transforms output voltage to relative units of dB input.

For each ith trace, an evaluation of the atmospheric extinction coefficient averaged over the effective range of received backscatter signal is derived from the slope $(\Delta S/\Delta R)$ of the linear least-squares fit to the $S_{i,j}$ versus R_j data. Two cases occur:

1) $\Delta S/\Delta R < 0$ (negative slope). In this case, a range-averaged value of the atmospheric extinction coefficient $(\bar{\sigma})$ is obtained from the relationship

$$\bar{\sigma} = \frac{1}{-8.7} \frac{\Delta S}{\Delta R} \quad ,$$

which is based on the assumption of atmospheric homogeneity. This assumption appears workable when operating within a fog such that the S-function sharply decreases with range due to the dominating effect of signal attenuation. Also, ΔR must represent the entire range interval over which the linear least-squares fit is applied. Small intervals of ΔR (< 25 m) must be avoided since they would give increasing weight to the presence of the small-scale inhomogeneities.

2) $\Delta S/\Delta R \geq 0$ (positive slope). In this case, the backscatter increases with range--i.e., the lidar beam penetrates a cloud or a fog of increasing density with range and an assumption of homogeneity is clearly invalid. For positive slope, values of atmospheric extinction coefficient are derived from the lidar data by an analysis based on an assumption of a β/σ relationship ($\beta = k_1 \sigma^{k_2}$) and a measured or estimated value of σ as an initial boundary condition* (see Collis et al., 1970).

Since the data-processing technique uses the slope of a linear least-squares fit to the data points in the computation of a range-averaged extinction coefficient, the technique is referred to as the "slope" method. Figures 5 and 6 show two samples of single-ended lidar data obtained during two different situations of low clouds and fog along the 15° slant path immediately adjacent to the elevated targets. The data were recorded by a low-sensitivity photomultiplier. Each sample includes the "raw" data in the form of Polaroid photographs of recorded oscilloscope traces of output voltage versus range, and the computer-processed data in the form of printouts of relative variations in the S-function versus range. The linear least-squares fit to the data points is indicated by a dashed line. On 2 August 1971 (Figure 5) a light fog was present, reducing the horizontal visibility to 1-2 km. A low-stratus ceiling extended downward almost

---

* In the present experiment, initial values of σ were obtained from Koschmieder's law and an estimate of visibility at the location of the lidar.

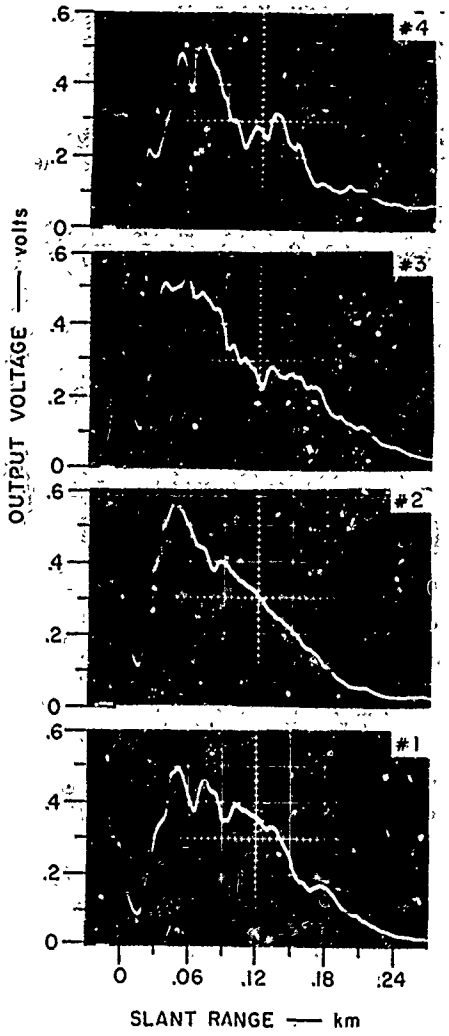

(a) RECORDED OSCILLOSCOPE TRACES OF OUTPUT VOLTAGE VERSUS RANGE

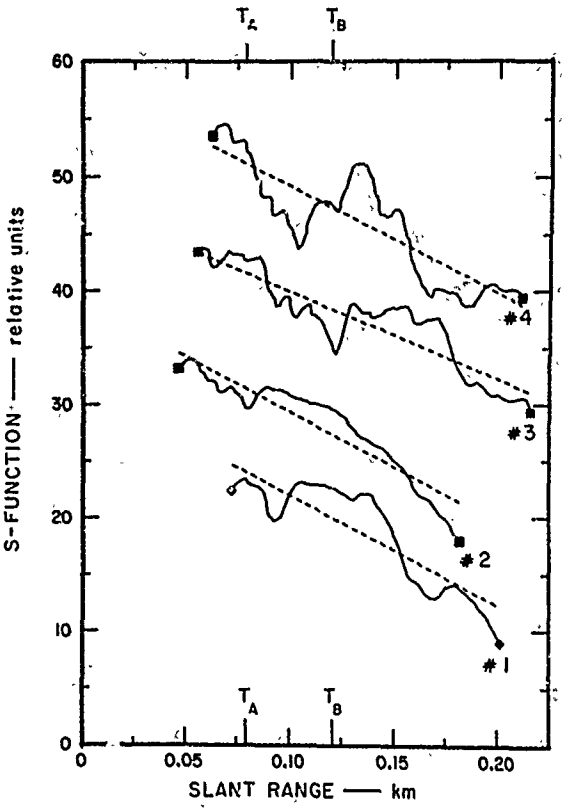

(b) COMPUTER-PROCESSED TRACES OF RELATIVE S-FUNCTION VERSUS RANGE. Traces are offset along the ordinate by 10 dB. Dashed line represents linear least-squares fit to the data points from a single trace.

FIGURE 5 SAMPLE OF SINGLE-ENDED LIDAR DATA OBTAINED ALONG 15° SLANT PATH DURING LOW CLOUDS AND FOG AT PILLAR POINT, CALIFORNIA, ON 2 AUGUST 1971

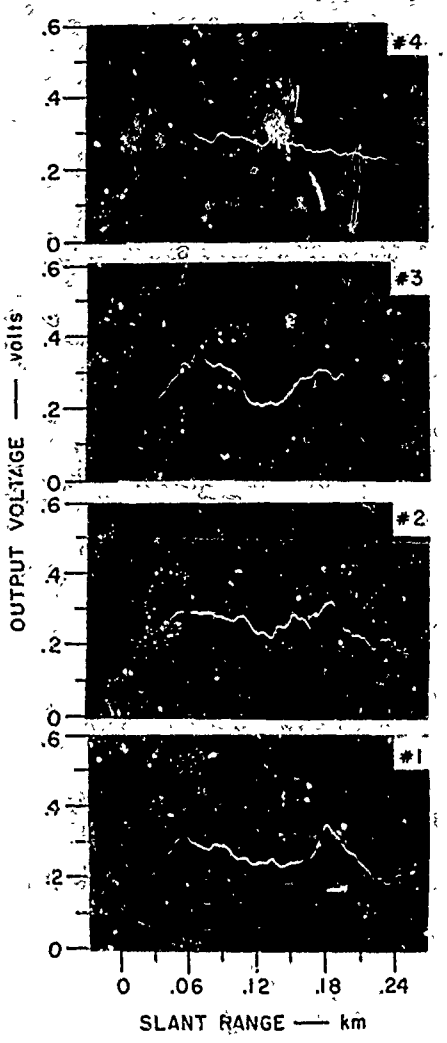

(a) RECORDED TRACES OF OUTPUT VOLTAGE VERSUS RANGE

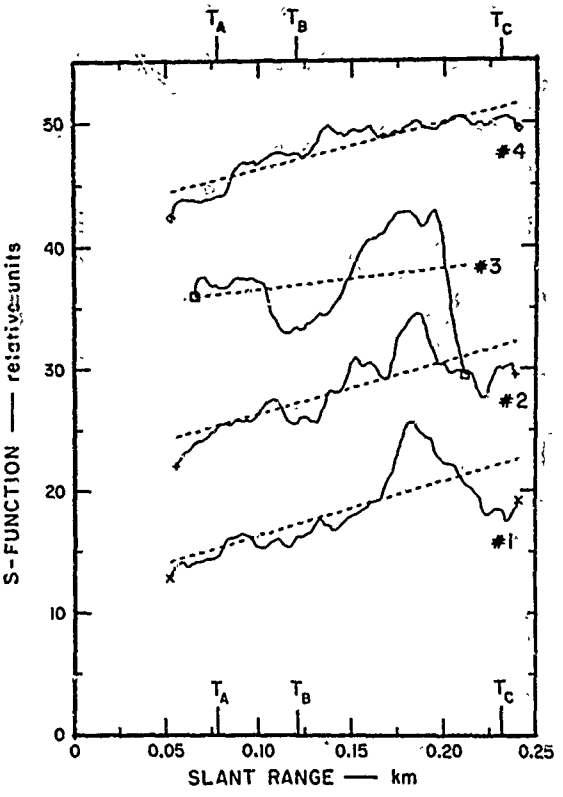

(b) COMPUTER-PROCESSED TRACES OF RELATIVE S-FUNCTION VERSUS RANGE. Traces are offset along the ordinate by 10 dB. Dashed line represents linear least-squares fit to the data points from a single trace.

FIGURE 6 SAMPLE OF SINGLE-ENDED LIDAR DATA OBTAINED ALONG 15° SLANT PATH DURING LOW-CEILING CONDITIONS AT PILLAR POINT, CALIFORNIA, ON 23 JULY 1971

to the ground. The first two targets (T_A and T_B) were clearly visible, but the highest (200-ft decision height) target, T_C, was only dimly visible due to obscuration by the low-stratus and fog. The linear fit to the computer-processed data [Figure 5(b)] shows that even though the fog is far from homogeneous, atmospheric extinction dominates the behavior of the lidar backscatter signal over the slant range of effective signal return ($\Delta S/\Delta R < 0$). On 23 July 1971 (Figure 6) all three elevated targets were clearly visible and below a well-defined but ragged ceiling of stratus clouds. The linear least-squares fits to the computer-processed lidar data of Figure 6(b) show an increase of the S-function with range ($\Delta S/\Delta R > 0$), owing to sharp increases in the atmospheric backscatter as the lidar beam points toward the cloud ceiling--i.e., into a scattering medium of increasing density with height.

C. Data Verification

No transmissometers or other visibility-measuring devices were available during the lidar/slant-visibility experiment at Pillar Point. Consequently, no evaluation of the validity and accuracy of the "slope" method is presented in terms of such measurements. However, previous research (Collis et al., 1970) demonstrated that atmospheric transmittance obtained from lidar/target data is highly correlated with the transmittance data from standard (type AN/GMQ 10) transmissometers. Therefore, extinction coefficients derived from the single-ended lidar data by the "slope" method are evaluated on the basis of a comparison with the extinction coefficients derived from the target-reflected signals. No point-to-point correlation between the single-ended data and the target data is possible because these data are not simultaneous but involve two lidar-pulse transmissions separated in time by 1 to 2 minutes. Because of the large natural fluctuations in visibility that occur in the very patchy coastal-fog con-

ditions encountered, this time difference is associated with large differences in the lidar data.

Values of range-averaged extinction coefficient obtained from the lidar data are also used to obtain slant visual range from the law of Koschmieder. The slant-visibility estimates thus obtained are compared with subjective visual observations of the three elevated targets made from the location of the lidar by the personnel operating the lidar.

D. Limitations of Data Analysis Technique

The linear least-squares procedure by means of which values of atmospheric extinction are derived from the lidar data can be applied to all lidar traces. However, the derived atmospheric extinction coefficients cannot be expected to be of equal validity. In other words, the present technique of deriving slant-range visibility from single-ended lidar data does not give operationally useful information under all conditions of fog and/or low clouds. Three situations were found to present difficulties.

Condition 1--During the onset of the advection-type fog that was encountered, fog patches could be observed to drift through the lidar's field of view at rapid speed. Figure 7 shows a series of four consecutive slant-path lidar traces of atmospheric backscatter signal versus range typical of these extremely inhomogeneous conditions. The traces, obtained at 1-minute intervals, show large variability in space and time. Although each individual trace can be processed by the "slope" method in order to obtain a value of atmospheric extinction, the validity of such a value cannot be assessed. Exactly how operationally useful information on slant visibility should be reported under these conditions has not been specified.

Condition 2--On 5 October 1971, a shallow layer of fog was observed with a well-defined upper boundary above which conditions were clear.

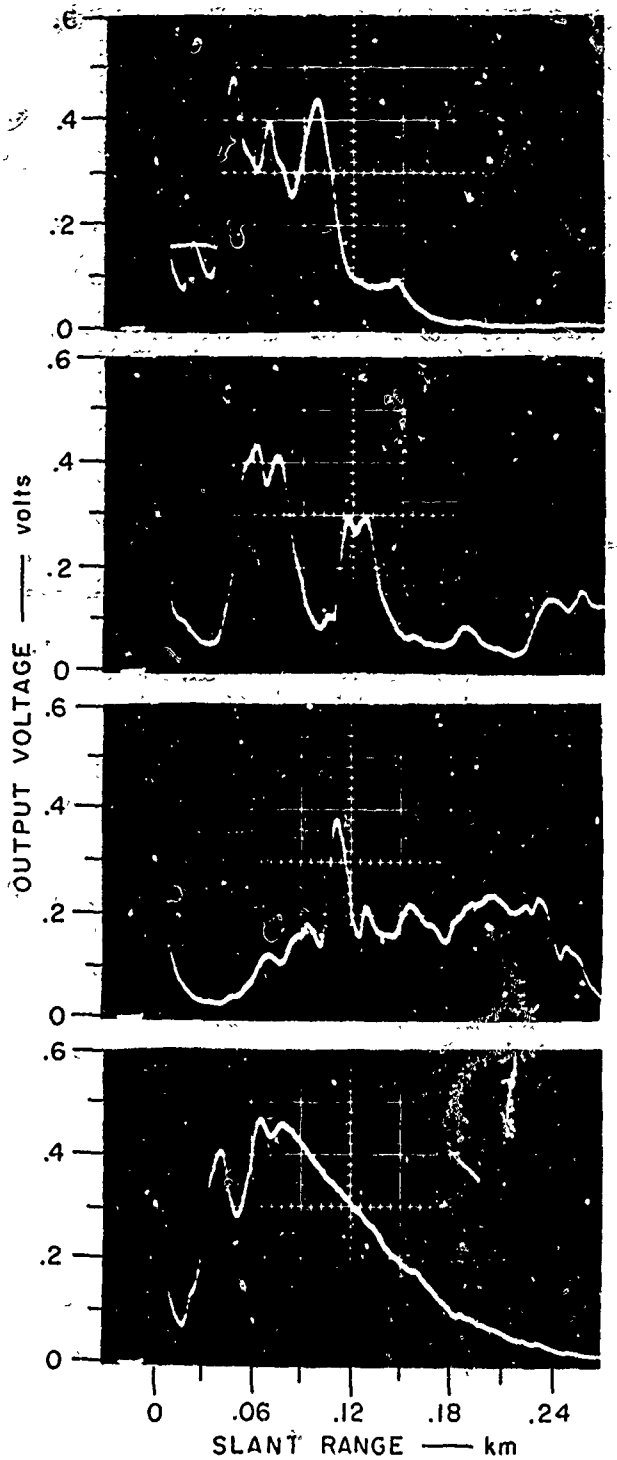

FIGURE 7 OSCILLOSCOPE TRACES OF LIDAR BACKSCATTER SIGNAL VERSUS RANGE RECORDED AT 1-MINUTE INTERVALS DURING THE ONSET OF ADVECTION-TYPE FOG AT PILLAR POINT, CALIFORNIA, ON 4 AUGUST 1971

In this case, the sharp decrease of signal intensity with range observed in the lidar data above the upper boundary of the fog cannot be included in the least-squares procedure since it does not relate to atmospheric extinction but to a sudden decrease in atmospheric backscatter with range as the lidar pulse exits from the fog into relatively clear air conditions. Figure 8 shows an example of these data recorded by the "gated" photomultiplier pmt 2 (gating distance 50 m) connected to the "new" logarithmic amplifier (logger 3). The upper fog-boundary can be clearly distinguished in the slant-range lidar traces.

Condition 3.--When a well-defined cloud ceiling is present at a height that intercepts the elevated lidar beam, the observed backscatter profile shows a sharp increase in atmospheric backscatter at the range corresponding to the cloud-base height. When the "slope" method is applied to this type of lidar trace, the linear least-squares procedure includes the data of the lower cloud boundary in averaging the signal variation with range, which significantly affects the slope of the linear fit. It has become evident from the collected lidar data that the backscatter signals from a cloud boundary should not be included when deriving values of range-averaged extinction coefficient and that the lidar trace should be processed in two parts, one part below the cloud base and the other part above the cloud base inside the cloud. Figure 9 illustrates the computer-processed data of relative variations in the S-function versus range representing four consecutive traces recorded 2 minutes apart along a slant path of 15° elevation. The data were obtained when rapid variations in the height of a low-stratus ceiling were observed and when the highest (200-ft decision height) target, T_C, was not visible. In Trace 3, the cloud ceiling was below the transmitted lidar beam and practically at ground level. In Traces 1, 2, and 4 the ceiling had suddenly risen and is intercepted by the elevated lidar beam. It is evident

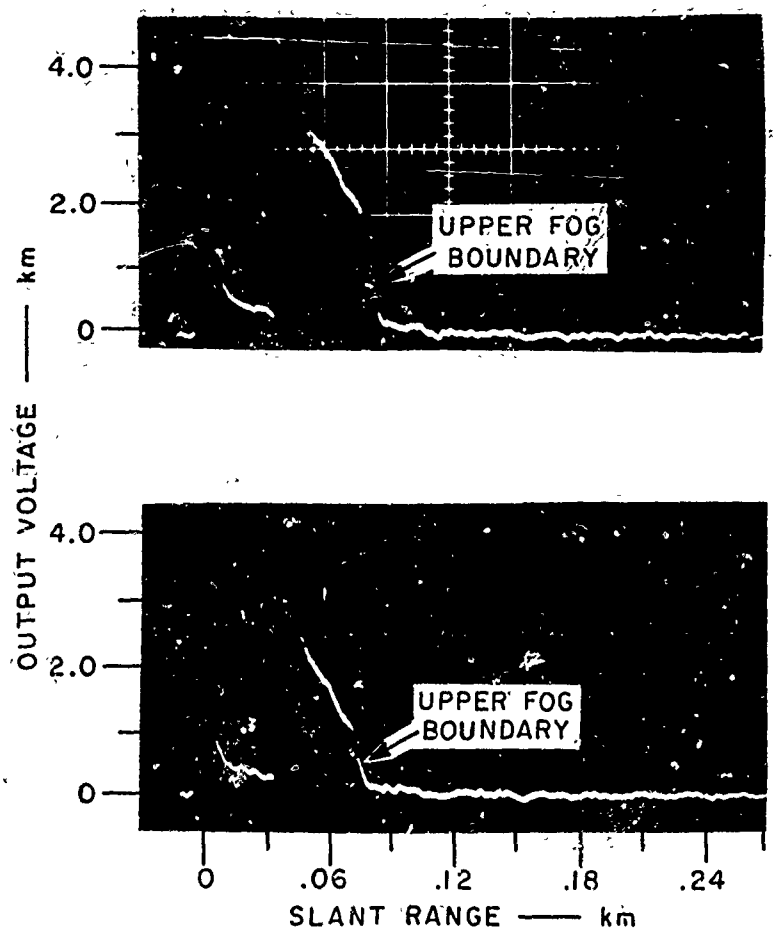

FIGURE 8 OSCILLOSCOPE TRACES OF LIDAR BACKSCATTER SIGNAL VERSUS RANGE RECORDED ALONG 15° SLANT PATH DURING SHALLOW FOG AT PILLAR POINT, CALIFORNIA, ON 5 OCTOBER 1971. Photomultiplier "gated off" for 0.3-μs duration.

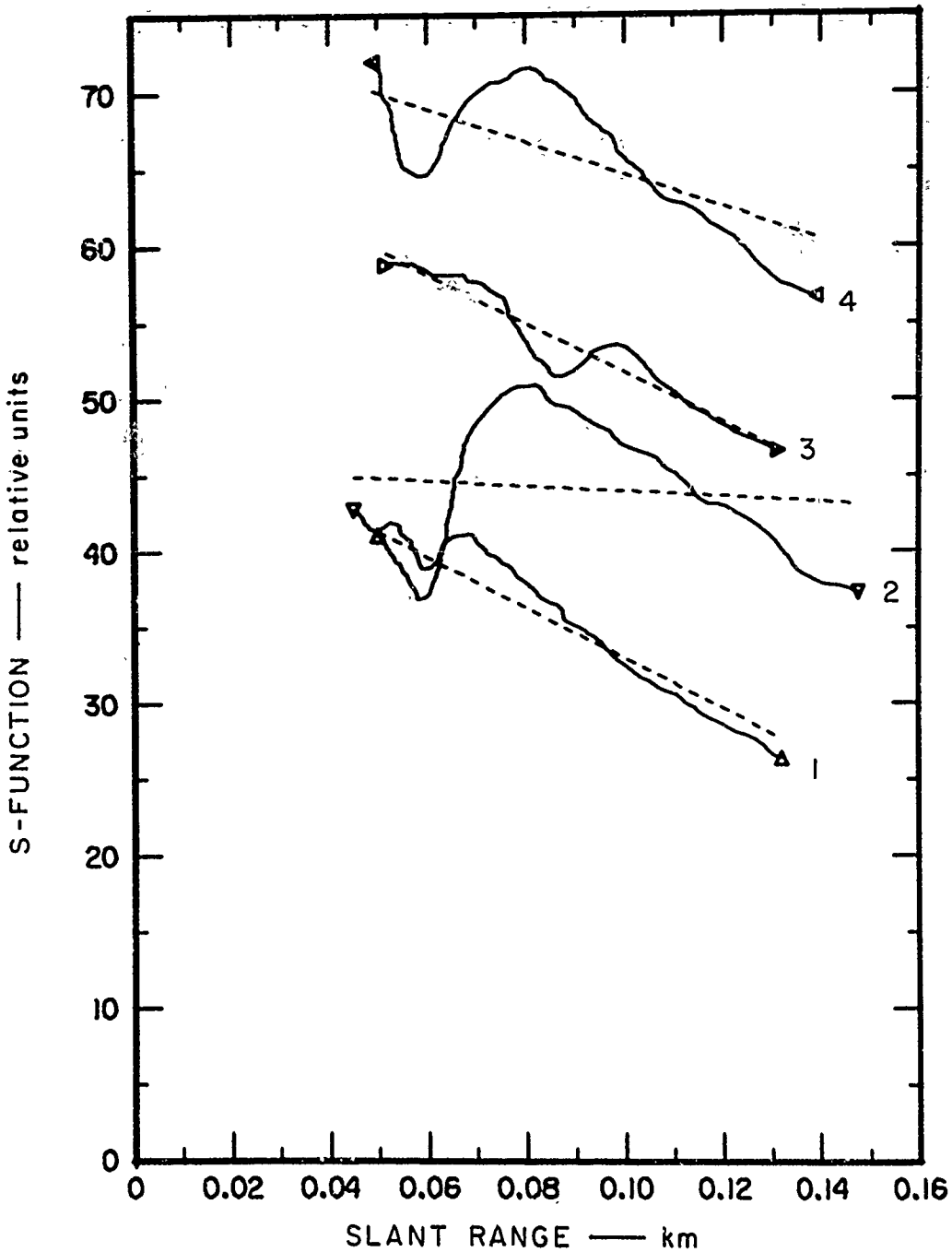

FIGURE 9 LIDAR TRACES OF RELATIVE S-FUNCTION VERSUS RANGE SHOWING EFFECT OF CLOUD CEILING ON SLOPE OF THE LINEAR LEAST-SQUARES FIT (Pillar Point, California, 19 July 1971)

that when the cloud ceiling is present in the lidar backscatter data, the linear least-squares fit to the data points gives a value of atmospheric extinction that is obviously invalid.

Although, in principle, the "slope" method can be applied to any lidar profile of atmospheric backscatter versus range observed during fog and low clouds, in practice, subjective judgment (human intelligence) is required to guide the analysis of the data and to assess the validity of the derived extinction coefficients. In the present study, both visual observations of the prevailing atmospheric conditions and inspection of the recorded Polaroid data were used to recognize and account for the three conditions described above. To what extent various subjective judgments can be expressed objectively and incorporated in a computer program remains to be determined. Under an additional task to the contract, an effort was made to identify Condition 3 by providing input information related to cloud-base height. The results are discussed later in this report.

V RESULTS OF OBSERVATIONAL PROGRAM

A. General

The field observation program can be divided into three separate periods on the basis of changes that were made in the logarithmic amplifiers of the dual receiver system with which the Mk V neodymium lidar was equipped. At the start of the program, the dual receiver system consisted of an upper (low-sensitivity) photomultiplier (pmt 1) connected to a logarithmic amplifier (logger 1) of known design and a lower ("gated") photomultiplier (pmt 2) connected to a logarithmic amplifier (logger 2) of similar design as logger 1 (see Section III, on Instrumentation and Equipment). The lidar/target data on slant visibility collected and analyzed during July and the beginning of August 1971 showed a consistent discrepancy in the output from these two pmt/logger components. Atmospheric extinction coefficients derived from the target data of pmt 2/logger 2 were too high as compared with those derived from the target data of pmt 1/logger 1 and also as compared to visual observations of the elevated targets. After various probable causes for the discrepancy were considered, a brief experiment revealed a large difference in the signal amplitude-bandwidth characteristics of the two log amplifiers. In fact, logger 2 appeared to pass low-intensity signals received from the passive reflectors with a considerable loss in signal intensity, which--under fog conditions--resulted in values of the atmospheric extinction coefficient that were too high. The log amplifier connected to the upper pmt (logger 1) displayed somewhat similar characteristics but much less severe, and derived values of atmospheric extinction appeared reasonable.

Since some uncertainty in the performance characteristics of logger 2 had been experienced during a previous field measurement program (see Collis et al., 1970), logger 2 was discarded and a prototype logarithmic amplifier of different design (logger 3) was installed on 17 August.

Because of the poor performance of logger 2 to which pmt 2 was originally connected, only the data from this receiver component collected on 19 July 1971 are presented in order to illustrate the discrepancy found in the extinction coefficients derived from the target data. All other data samples presented for July and August are those recorded from the receiver component pmt 1/logger 1. The characteristics of logger 3 were tested under various fog conditions from 17 August to 14 September. Observations of slant visibility using a dual receiver system consisting of pmt 1 connected to logger 1 and pmt 2 connected to logger 3 were resumed on 5 October. An extensive record of data collected simultaneously with two photomultipliers is presented for 13 October.

Table 2 lists the slant-path lidar observations that were made during the three separate periods. A total of 22-1/2 hours of lidar-transmission time was used to collect the data. Various data samples were collected for the purpose of testing equipment components and operational procedures. The data from six separate observation periods covering various degrees of fog and low cloud conditions are presented in detail.

B. Presentation of Data Samples

1. 19 July 1971 (Horizontal Visibility 600-1200 m)

The first series of slant-path lidar observations was made on 19 July 1971 when a dense fog enveloped the Pillar Point field site. The fog was associated with low-level stratus clouds. The lowest target, T_A, remained visible at all times, but target T_B (100-ft decision height) occasionally disappeared from sight. The highest (200-ft decision

height) target, T_C, was never visible. Because of a failure in the power supply of the upper photomultiplier (pmt 1) of the dual receiver system, only data from the lower "gated" photomultiplier (pmt 2) were available.

Figure 10 shows an example of recorded data. The oscilloscope traces of signal intensity versus range are gated on at a range of 50-60 meters in order to avoid receiver saturation by the high-intensity backscatter signals from close range. The target data [Figure 10(a)] show no return from T_C and the near-disappearance of the reflected signal from T_B. The single-ended data [Figure 10(b)] show the effects of strong attenuation with range in the backscatter signal from the atmosphere itself.

In Figure 11, atmospheric extinction coefficients obtained from the target data (dots connected by solid lines) and from the single-ended data (crosses connected by dashed lines) are compared for a 50-minute period of observation. The data were collected by firing the lidar "on and off" the elevated targets at intervals of 1 minute. A 1-minute time interval was required to change the azimuth of the lidar and the neutral density filters in front of the photomultiplier. Measured values of the extinction coefficient are connected by straight lines in order to show the large temporal fluctuations in atmospheric extinction that are characteristic of coastal fog conditions.

To compare the lidar measurements with visual observations made of the elevated targets, a special visual-range scale is drawn alongside the lidar data of Figure 11. Using the lidar-observed extinction coefficients (σ), corresponding values of slant visual range (V) are obtained from Koschmieder's law $\varepsilon_o = \exp(-\sigma V)$ using two different values for the contrast threshold ε_o (see Hering et al., 1971). The locations of the elevated targets are indicated at their appropriate slant-range distances from the location of the lidar--i.e., from the point where the visibility

Table 2

SUMMARY OF SLANT-RANGE VISIBILITY MEASUREMENTS MADE BY LIDAR AT PILLAR POINT, CALIFORNIA

Date (1971)	Time Period of Observation (PDT)	Number of Observations		Description of Observations	Observed Visibility in Direction of Targets	
		Target Data	Single-ended Data		Horizontal (m)	Slant Range
Dual Receiver System with pmt 1/logger 1 and pmt 2/logger 2						
19 July	15:30-16:30	25	27	On and off 15° elevated targets	600-1200	T_A - Visible T_B - Occasionally obscured T_C - Not visible
23 July	08:17-10:19	19	20	Angular scanning from 15° targets to horizontal targets	4000-6000	All elevated targets below cloud base
	11:15-11:50	17	17	On and off 15° elevated targets	4000-8000	
	12:05-12:37	16	15	On and off horizontal targets	6000-8000	
2 August	09:35-10:35	31	31	On and off 15° elevated targets	1000-2000	T_A - Visible T_B - Visible T_C - Obscured most of time
	11:08-11:54	22	24	On and off 15° elevated targets	1000-2000	T_A - Visible T_B - Visible T_C - In and out of cloud base
4 August	08:50-09:25	13	22	Angular scanning from 15° targets to horizontal targets	600-800	Passage of fog bank
	10:00-11:30	45	--	15° target calibration	10-15 km	All targets visible
	12:00-12:30	30	--	Horizontal target calibration	10-15 km	
	13:40-14:25	19	19	On and off 15° elevated targets	≥1000	T_A - Visible T_B - Visible T_C - Not visible most of time

Table 2 (Concluded)

Date (1971)	Time Period of Observation (PDT)	Number of Observations		Description of Observations	Observed Visibility in Direction of Targets	
		Target Data	Single-ended Data		Horizontal (m)	Slant Range
Testing of Prototype logger 3						
17 August	13:00-14:00	20	--	On 15° elevated targets	4000-8000	All targets below cloud base
	14:00-15:30	12	10	On horizontal targets	4000-8000	
	15:30-16:30	--	--	Cloud ceiling measurements with mirror	4000-8000	
18 August	Recalibration of All Logarithmic Amplifiers in the Laboratory					
3 September	11:00-12:00	20	--	15° target calibration	4000-8000	Clear
	12:00-13:00	23	--	Horizontal target calibration	4000-8000	Clear
14 September	Field Experiment to Collect Data on Bandwidth Characteristics of Loggers 1, 2, and 3.					
	Dual Receiver System with pmt 1/logger 1 and pmt 2/logger 3					
5 October	15:00-18:00	20	15	On and off 15° elevated targets	70-100	T_A - Visible T_B - Occasionally visible
		15	10	On and off horizontal targets		T_C - Not visible
13 October	10:22-14:07	51	47	On and off 15° elevated targets and cloud ceiling measurements with mirror	500-800	T_A - Visible T_B - Occasionally visible T_C - Occasionally visible
15 November	12:00-13:00	33	--	15° target calibration	10,000-20,000	All targets visible

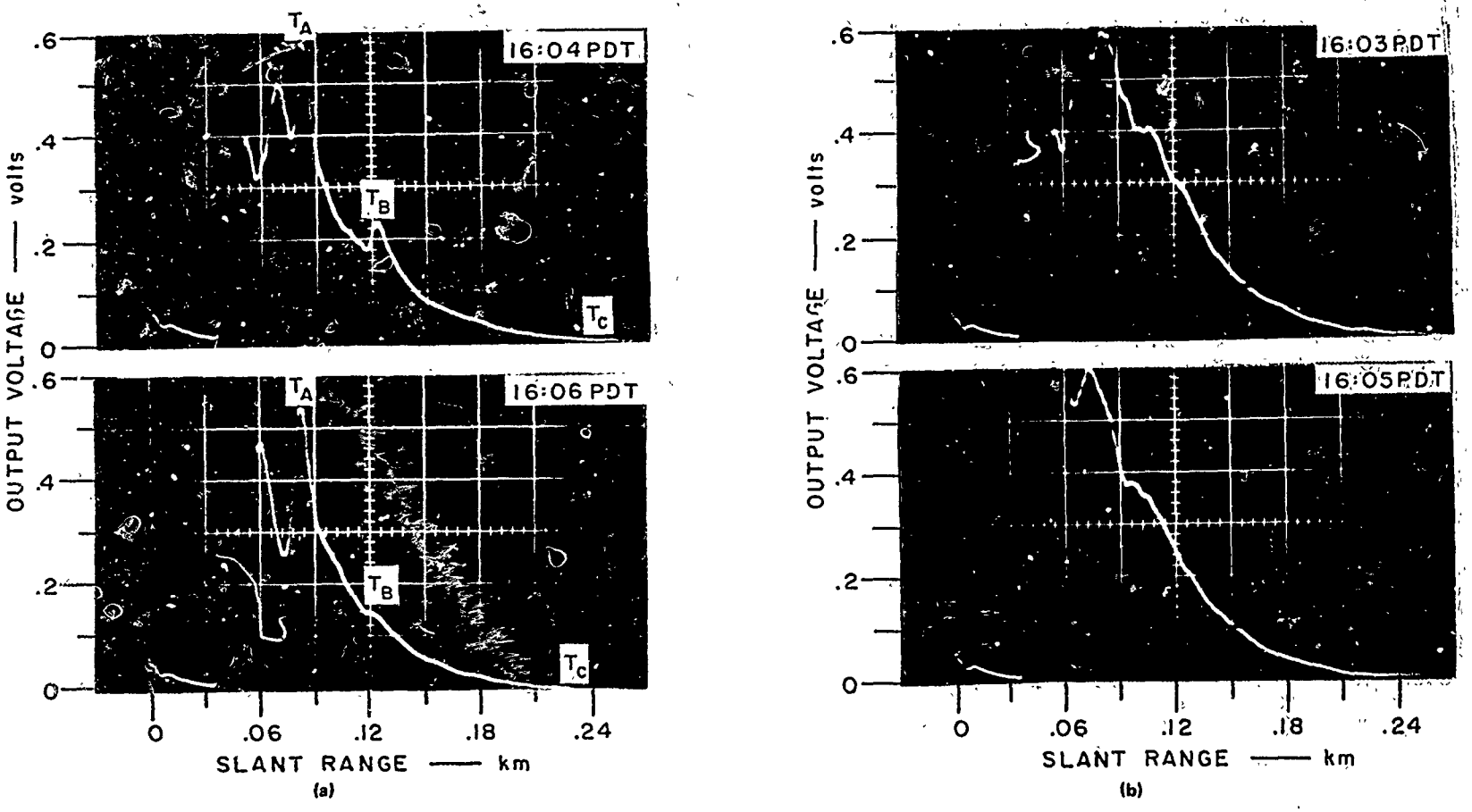

FIGURE 10 PHOTOGRAPHS OF OSCILLOSCOPE DISPLAY SHOWING (a) 15° ELEVATED-TARGET DATA AND (b) 15° SLANT-PATH SINGLE-ENDED DATA RECORDED DURING LOW CLOUDS AND FOG ON 19 JULY 1971

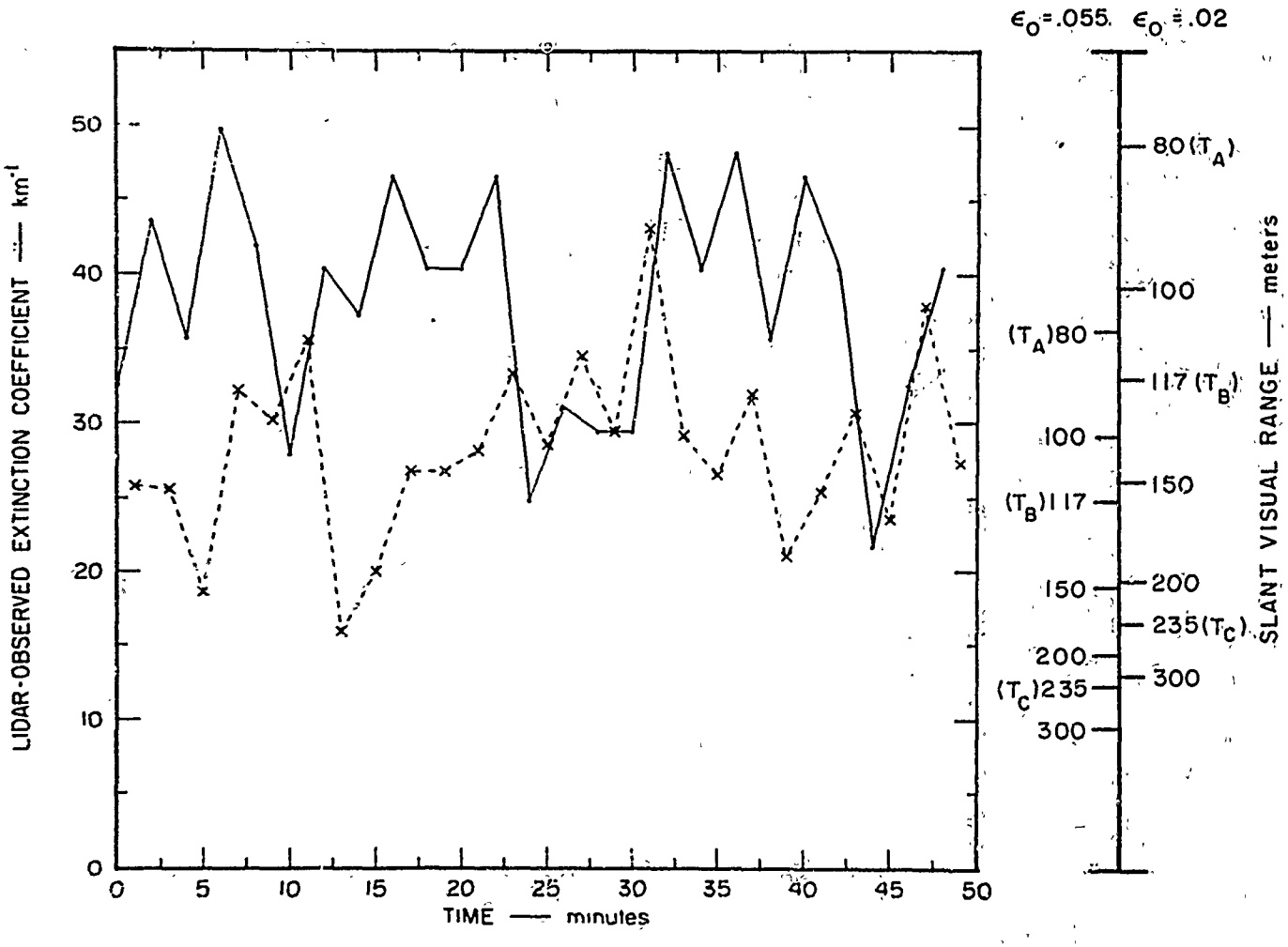

FIGURE 11 TIME SERIES OF SLANT-PATH ATMOSPHERIC EXTINCTION COEFFICIENT AND CORRESPONDING SLANT VISUAL RANGE MEASURED BY LIDAR DURING LOW CLOUDS AND FOG ON 19 JULY 1971, 15:30-16:20 PDT. Target data—dots and solid lines, single-ended data—crosses and dashed lines.

of the targets was assessed. Both the target data and the single-ended data correspond to slant visibilities that are less than the slant-range distance of 235 meters required to see the 200-ft decision height target, T_C, from the location of the lidar. Thus, both the target data and the single-ended lidar data correctly predict the obscuration of T_C. However, extinction coefficients derived from the target data correspond to slant visibilities that (1) are less than the slant range of 117 meters required to observe visually the 100-ft decision-height target, T_B, and (2) approach the slant range of 80 meters required to observe target T_A. Except for an occasional obscuration of T_B, both T_A and T_B remained visible throughout the observation period. As mentioned above, this discrepancy in the target data was traced to a bias in the bandwidth characteristics of logger 2.

The actual conditions as they were observed are well represented by the single-ended lidar data, especially when corresponding slant visibilities are based on $\epsilon_o = 0.02$. Slant visibilities deduced from the single-ended lidar data using a contrast threshold $\epsilon_o = 0.055$ are too low compared to what was actually observed. For example, not only would target T_B have been totally obscured but the lowest target, T_A, would have disappeared from sight two or three times during the 50-minute observation period. Both T_A and T_B remained visible from the location of the lidar.

Figure 11 demonstrates that a single measurement of slant visual range has little or no significance because of the large temporal fluctuations. However, useful information on slant-visibility conditions can be obtained from the 50-minute time-series of single-transmission measurements. Using the total sample (27 measurements) of extinction coefficients derived from the single-ended data, Figure 12 shows the percentage frequency with which values of slant-range visibility were measured by the lidar, using the contrast threshold $\epsilon_o = 0.02$. In the

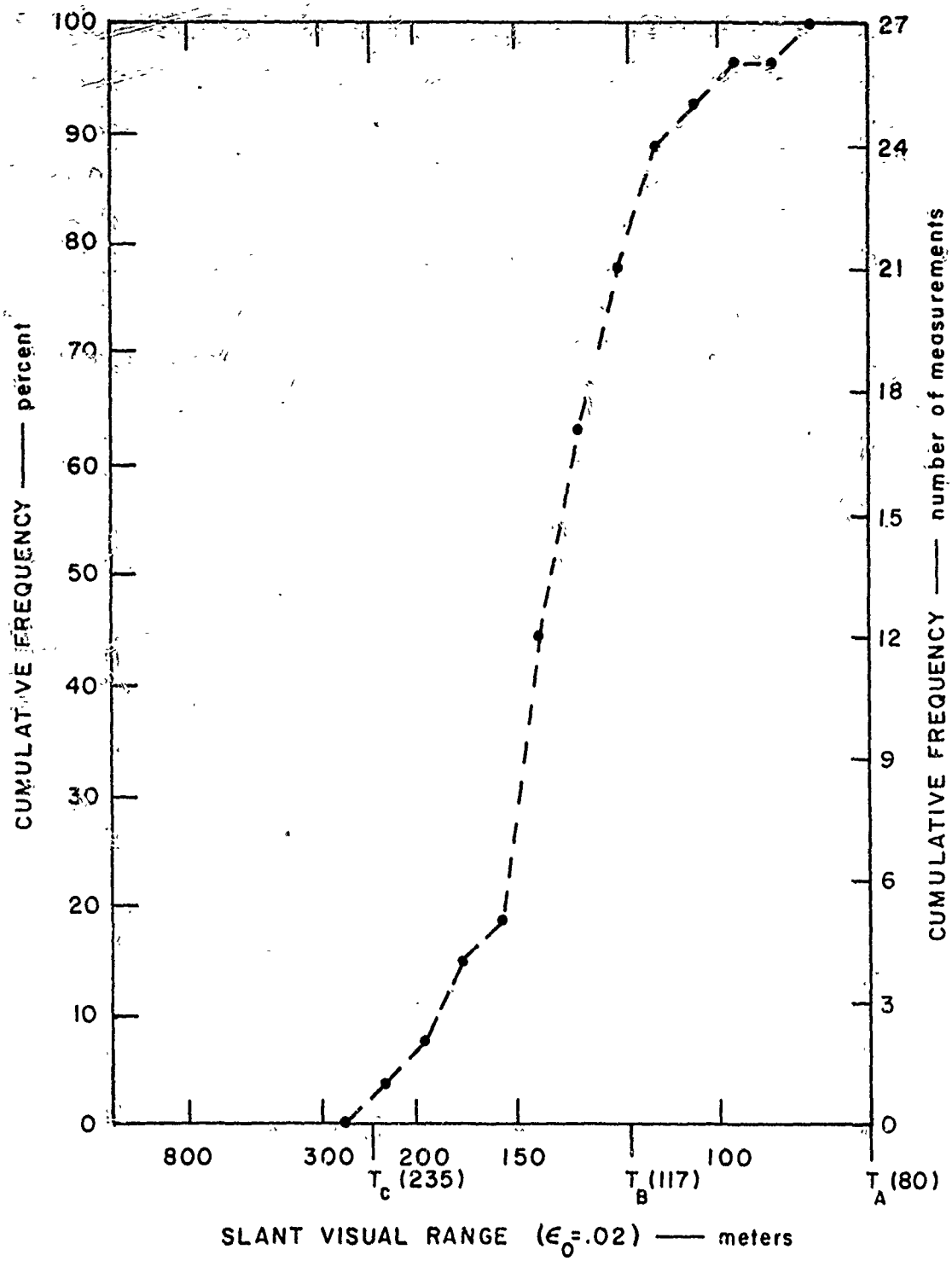

FIGURE 12 CUMULATIVE FREQUENCY OF SLANT VISUAL RANGE MEASURED BY LIDAR DURING LOW CLOUDS AND FOG ON 19 JULY 1971, 15:30-16:20 PDT

27 measurements can be considered as a sample from an infinitely large population of measurements representing the prevailing fog condition, it is concluded that the lidar data predict that (1) 100 percent of the time, the slant visual range was less than the 235 meters required to see the ground (the location of the lidar) along the 15° line of sight from the cockpit at the 200-ft decision height (T_C not visible from the location of the lidar) and (2) 80 percent of the time, the slant visual range was adequate to see the ground along the 15° line of sight from the cockpit at the 100-ft decision height (T_B visible from the location of the lidar). These predicted conditions closely resemble the actual conditions as they were evaluated from the ground on the basis of target visibility.

2. 23 July 1971 (Horizontal Visibility 4000-8000 m)

On 23 July, a low, ragged ceiling of stratus clouds was observed with horizontal visibility of 4 to 8 km. The two lowest targets, T_A and T_B, were clearly visible, but the highest (200-ft decision height) target, T_C, was just below the stratus clouds and became occasionally obscured by the ragged cloud base.

Slant-path lidar observations of the elevated targets and of the atmospheric backscatter were made for a period of 35 minutes (11:15-11:50 PDT), using the dual receiver system consisting of pmt 2/logger 2 and pmt 1/logger 1. Because of the bias discovered in logger 2, only the data from the low-sensitivity photomultiplier (pmt 1) are presented. Figure 13 shows an example of four single-ended traces of atmospheric backscatter signal versus range obtained at intervals of 2 minutes along the 15° slant path adjacent to the elevated targets. The traces, which present the relative variations of the S-function versus slant range, are printed along the ordinate with a 10-dB offset. Values of atmospheric extinction coefficient computed from the linear least-squares fit to the

data points are indicated next to each trace. The large increase in atmospheric backscatter with range shown in Traces 1 and 2 at a range of 200 m suggests the presence of a cloud ceiling at that point. This cloud ceiling may have dropped to a lower height in Traces 3 and 4. Exactly at what height the cloud base would have been measured is not known since no vertically pointing ceiling-measuring device was available.*

It is obvious that, especially in the case of Trace 3, the linear fit to the data points does not accurately describe the slope of the trace. In fact, whenever a boundary of large inhomogeneity such as a lower cloud boundary is present in the data, the least-squares averaging process should not be carried across this boundary. Instead, the lidar trace should be divided into two parts at the point where on the basis of the maximum increase of atmospheric backscatter with range the cloud base could be located.

The 17 traces of atmospheric backscatter versus range that were collected were analyzed in two ways. Firstly, the linear least-squares fit was drawn to the data points of the entire trace, as shown in Figure 13, regardless of the presence of cloud boundaries. Secondly, the traces were reanalyzed by dividing every trace that indicated the presence of a cloud boundary into two parts on a subjective basis, and applying the least-squares procedure separately to each part. Figure 14 illustrates how the lidar traces of Figure 13 were reanalyzed. Recombination of the extinction coefficients computed for the part below the estimated cloud base [Figure 14(a)] and above the estimated cloud base [Figure 14(b)] of each trace gives the values shown in parentheses

---

* Because of its location in the van and its fixed configuration for 15° slant-range observations, at this time the lidar could not be pointed vertically for accurate measurements of cloud-base height.

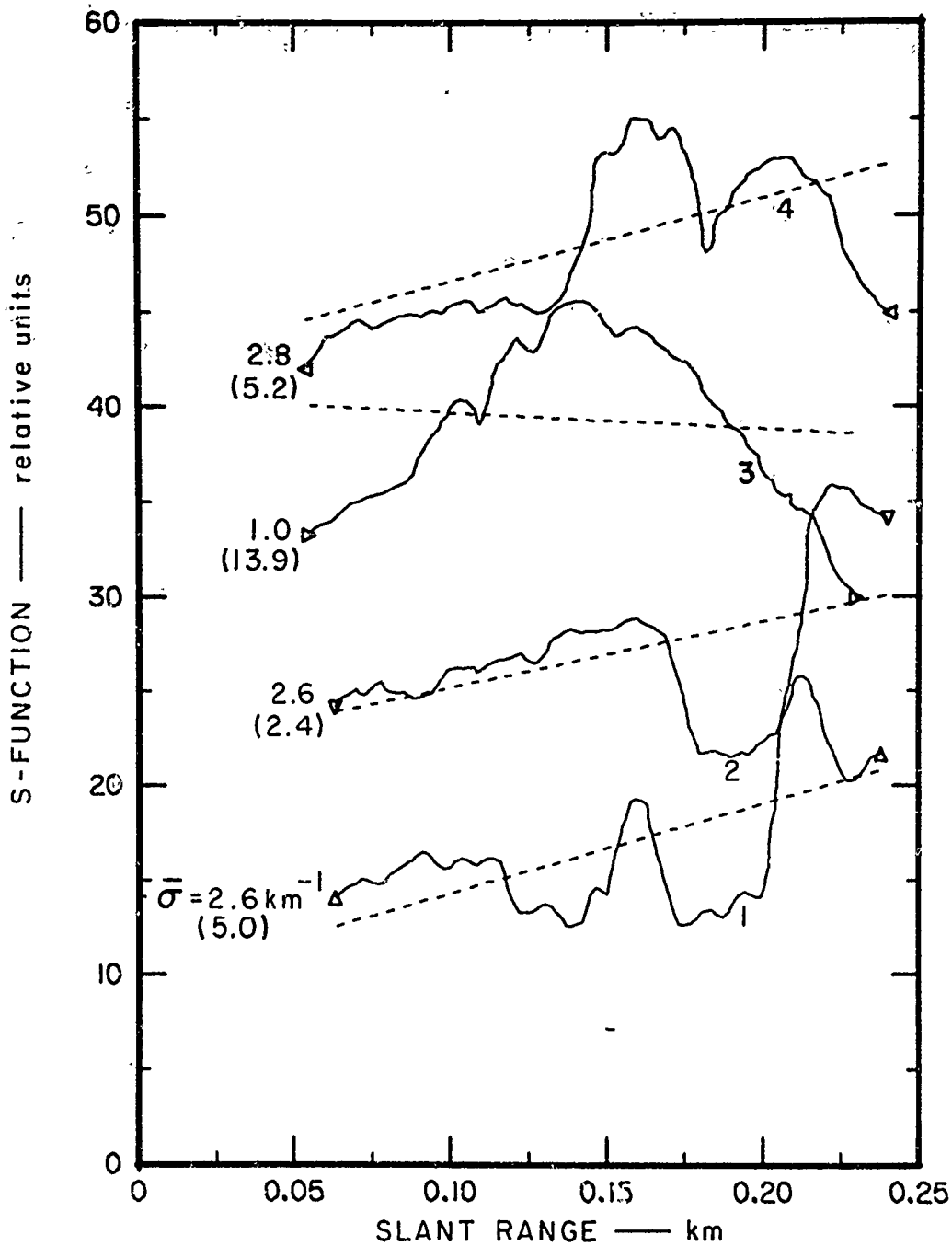

FIGURE 13 LIDAR TRACES OF RELATIVE S-FUNCTION VERSUS RANGE OBTAINED AT 2-MINUTE INTERVALS ALONG 15° SLANT PATH DURING THE PRESENCE OF LOW STRATUS CLOUDS ON 23 JULY 1971

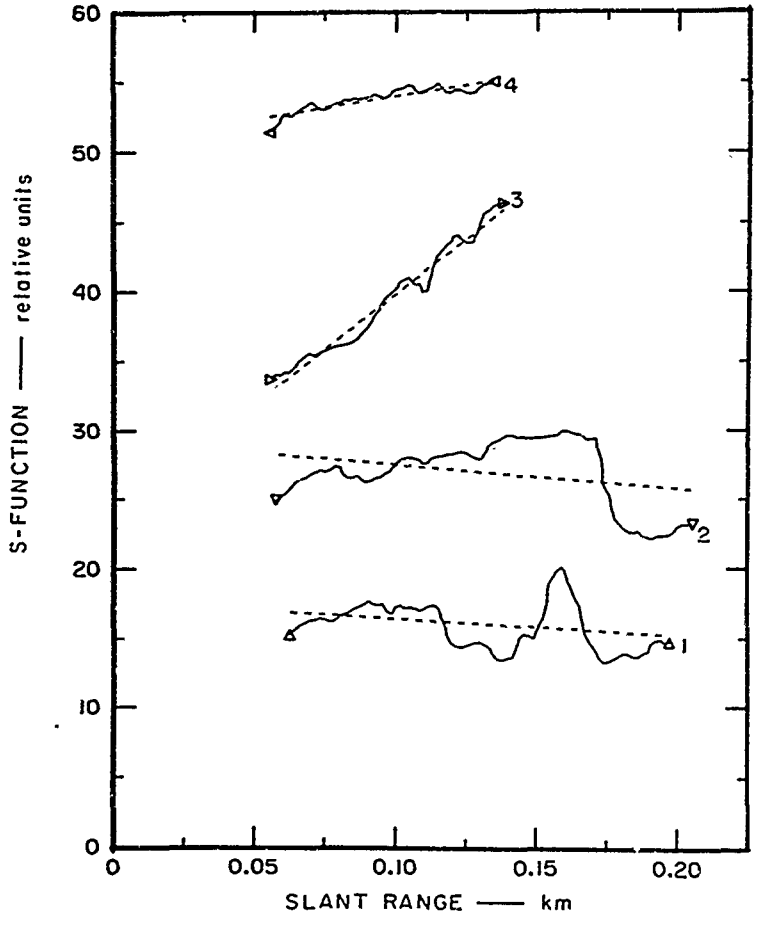

(a) REANALYSIS OF TRACES BELOW PROBABLE CLOUD BASE

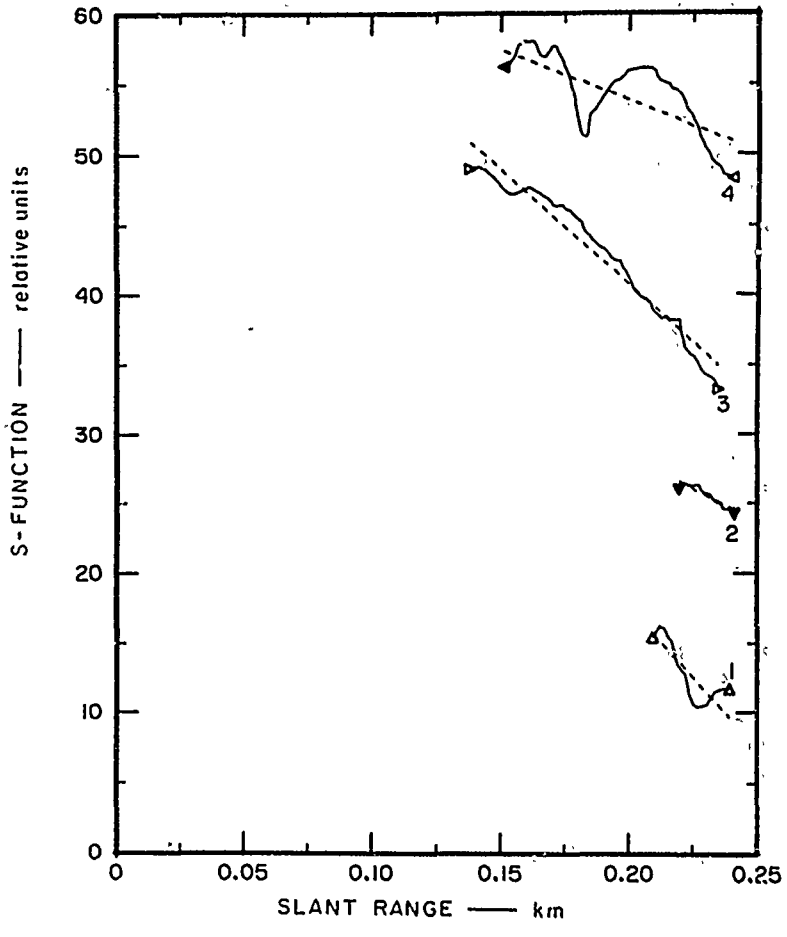

(b) REANALYSIS OF TRACES ABOVE PROBABLE CLOUD BASE. Recombination of (a) and (b) gives improved values of atmospheric extinction coefficient for each trace (shown between parentheses in Figure 12).

FIGURE 14 LIDAR TRACES OF FIGURE 12 REANALYZED TO ACCOUNT FOR PRESENCE OF CLOUD CEILING

alongside the traces of Figure 13. A large positive improvement results for Trace 3. At the time this trace was recorded, target T_C was obscured. The recomputed extinction coefficient ($13.9\ km^{-1}$) corresponds to a visual slant range of 280 m ($\epsilon_o = 0.02$), which is just beyond the slant-range distance of T_C (235 m).

Figure 15 shows the variation with time of the atmospheric extinction coefficients derived from the reflected signals of the three elevated targets. Solid lines connect the extinction coefficients measured over the slant-path distance from T_A to T_B--i.e.,

$$\bar{\sigma}_{T_A,T_B} = \frac{1}{R_B - R_A} \int_{R_A}^{R_B} \sigma \, dR \quad .$$

Dashed lines connect the extinction coefficients measured over the slant-path distance from T_B to T_C--i.e.,

$$\bar{\sigma}_{T_B,T_C} = \frac{1}{R_C - R_B} \int_{R_B}^{R_C} \sigma \, dR \quad .$$

The position of the dashed line relative to the solid line reflects the increase in $\bar{\sigma}$ with slant range toward the base of the stratus clouds and also shows the tendency toward large variations in atmospheric extinction immediately under the cloud base near the 200-ft decision height. These variations are most likely associated with the ragged appearance of the cloud base. The occasional tendency for the obscuration of T_C from sight as well as the good visibility conditions below the 200-ft decision height are reflected by the lidar/target data.

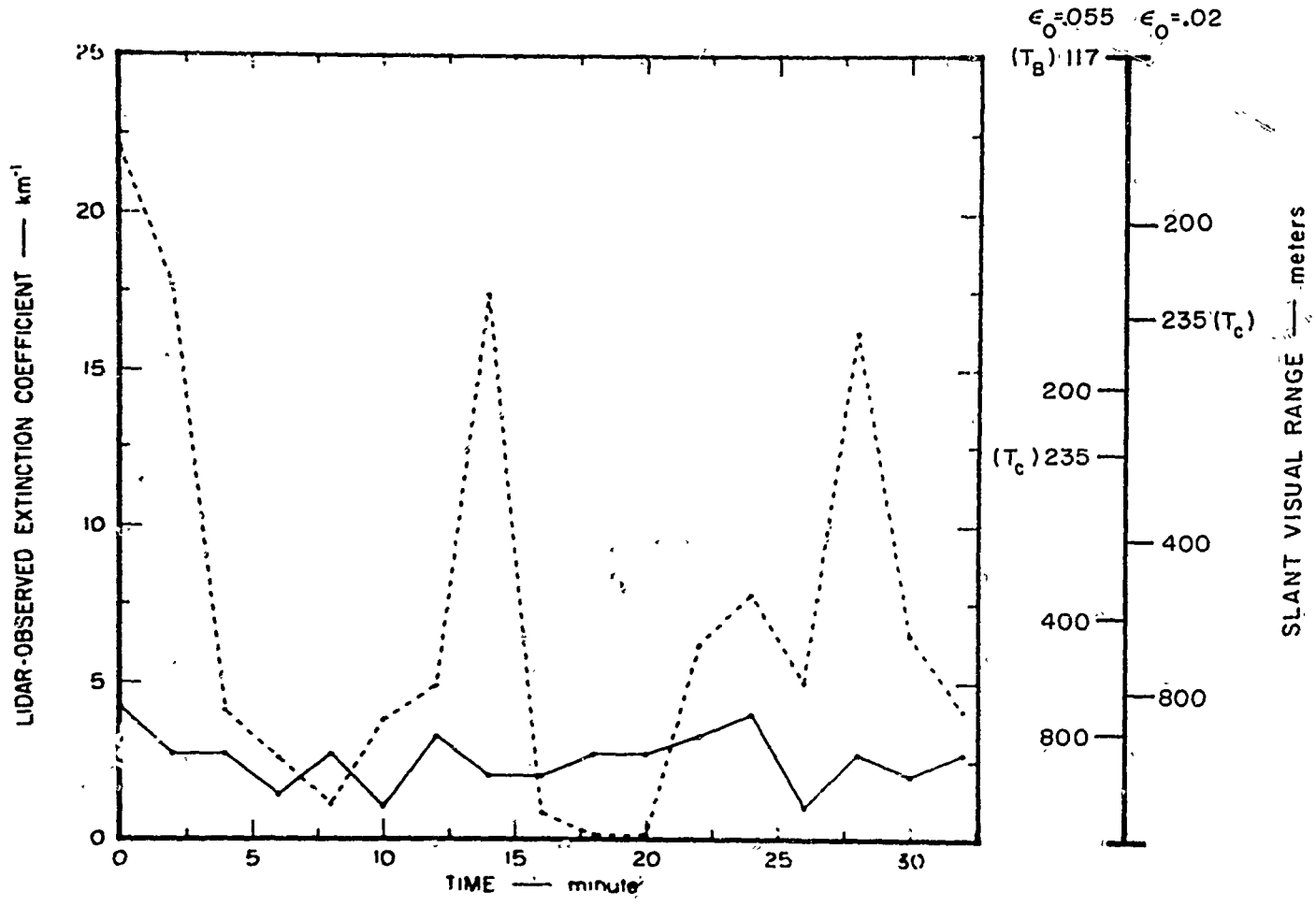

FIGURE 15 TIME VARIATION OF THE ATMOSPHERIC EXTINCTION COEFFICIENT AVERAGED OVER THE 15° SLANT-PATH DISTANCE FROM TARGET T_A TO T_B (Solid Line) AND FROM T_B TO T_C (Dashed Line) OBSERVED BY LIDAR DURING LOW CLOUDS AT PILLAR POINT, CALIFORNIA, ON 23 JULY 1971

Figure 16 compares target-derived extinction coefficients with those computed from the single-ended data by the "slope" method. The target data (dots connected by solid lines) represent the extinction coefficients averaged over the slant-path distance from T_A to T_C (154 m); these can be obtained from the data of Figure 15 as follows:

$$\bar{\sigma}_{T_A,T_C} = \frac{1}{R_C - R_A}\left\{\int_{R_A}^{R_B} \sigma\, dR + \int_{R_B}^{R_C} \sigma\, dR\right\}$$

$$= \frac{1}{R_C - R_A}\left\{\bar{\sigma}_{T_A,T_B}(R_B - R_A) + \bar{\sigma}_{T_B,T_C}(R_C - R_B)\right\} .$$

In Figure 16(a), the atmospheric extinction coefficients derived from the single-ended lidar data (crosses joined by dashed lines) were obtained by applying the linear least-squares procedure to the data points of the entire trace in the manner illustrated in Figure 13. In Figure 16(b), the extinction coefficients were computed from the single-ended data by applying the linear least-squares procedure separately to the traces above and below the apparent cloud ceiling in the manner illustrated in Figure 14. It is seen that agreement with the target data is greatly improved when cloud-base height is considered in the analysis of the single-ended data. The numbered points in Figure 16 are those related to the traces of Figures 13 and 14.

The data analysis of 23 July demonstrates that the "slope" technique should not be applied indiscriminately to the single-ended lidar data but that results can be greatly improved by identifying and accounting for the presence of a lower cloud boundary. Thus, information on cloud-base height appears to be desirable input to our present technique of deriving slant visibility from single-ended lidar observations.

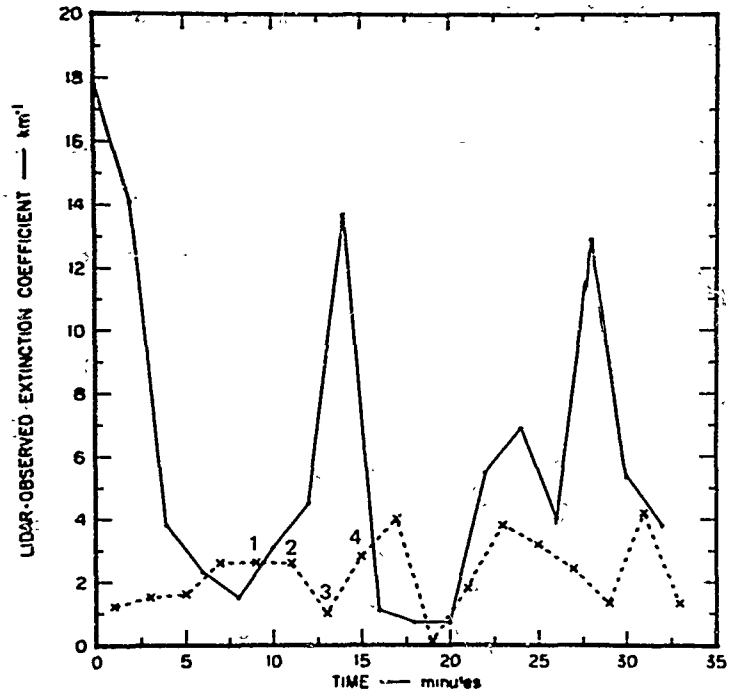

(a) CLOUD CEILING NOT CONSIDERED IN DATA ANALYSIS

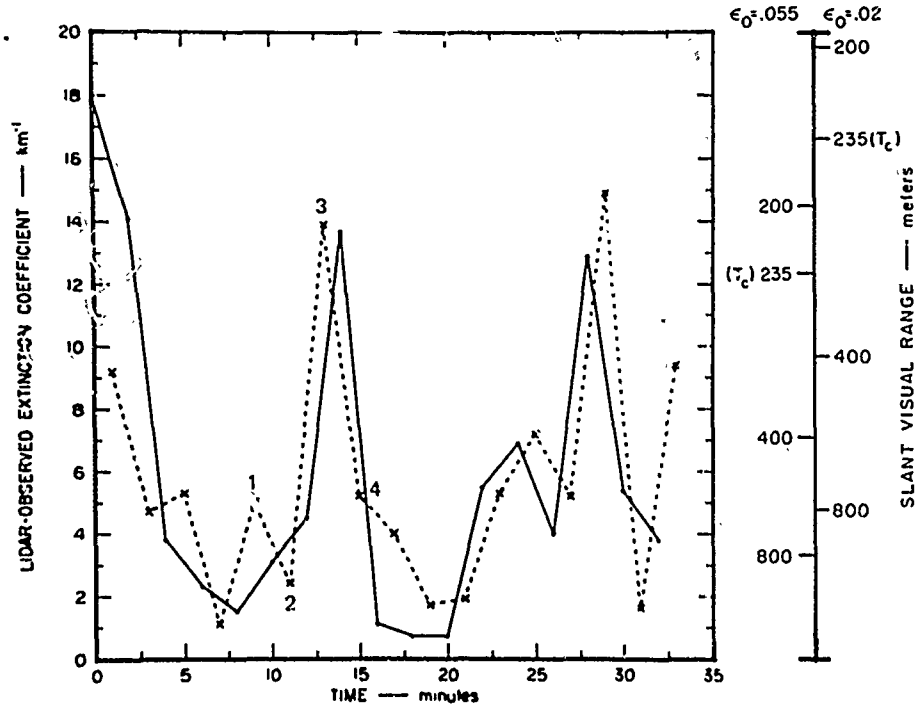

(b) CLOUD CEILING CONSIDERED IN DATA ANALYSIS

FIGURE 16 COMPARISON BETWEEN SLANT-PATH ATMOSPHERIC EXTINCTION COEFFICIENTS DERIVED FROM TARGET DATA (Dots and Solid Lines) AND FROM SINGLE-ENDED LIDAR DATA (Crosses and Dashed Lines)

3. 2 August 1971 (Horizontal Visibility 1000-2000 m)

On 2 August, a light fog was present that reduced the horizontal visibility to 1-2 km. A low stratus ceiling extended downward almost to the ground. Slant-range target data and single-ended data were collected from 09:35-10:35 PDT and from 11:08-11:54 PDT. During the first time period, the 200-ft-decision height target, T_C, was obscured to the extent that a record of its reflected signal could not be obtained. During the second period, the stratus had lifted somewhat and T_C was visually observed "in and out" of the cloud base. Targets T_A and T_B were always visible.

Figure 17(a) shows an example of computer-processed single-ended lidar data obtained along a 15° slant path at intervals of about 2 minutes during the first period of observation. The linear least-squares fit to the data points of each trace suggests that, on the average, atmospheric extinction controls the behavior of the lidar backscatter signal with range ($\Delta S/\Delta R < 0$). Because of the rapid extinction of the lidar-pulse energy in the dense stratus clouds, the data do not extend much more than 10-20 m beyond the slant range of target T_B. Figure 17(b) compares the atmospheric extinction coefficients obtained from the target data (dots connected by solid lines) and from the single-ended data (crosses connected by dashed lines). Because of the frequent obscuration of T_C, the target data only provide extinction coefficients averaged over the slant-path distance from T_A to T_B (37-m slant-range distance). The single-ended data are analyzed by the least-squares procedure in the manner illustrated in Figure 17(a). It is seen from the slant visual-range scale that the target data correctly predict frequent obscuration of T_C (both for $\epsilon_o = 0.055$ and for $\epsilon_o = 0.02$)--i.e., slant visibilities corresponding to many of the target-derived extinction coefficients are less than those required to observe T_C (235-m slant-range distance from the lidar). However, only for $\epsilon_o = 0.02$ do the target data reproduce

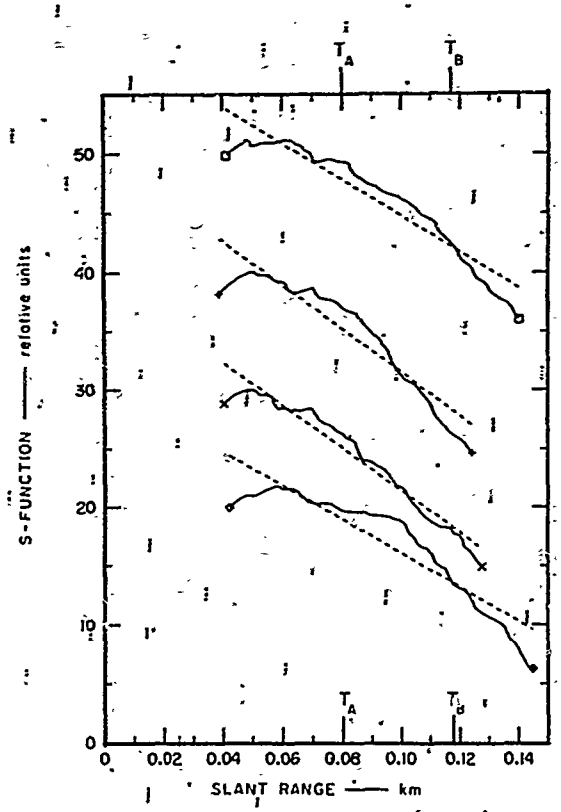

(a) SAMPLE OF SINGLE-ENDED LIDAR TRACES OBTAINED ALONG 15° SLANT PATH DURING LOW CLOUDS AND FOG ON 2 AUGUST 1971

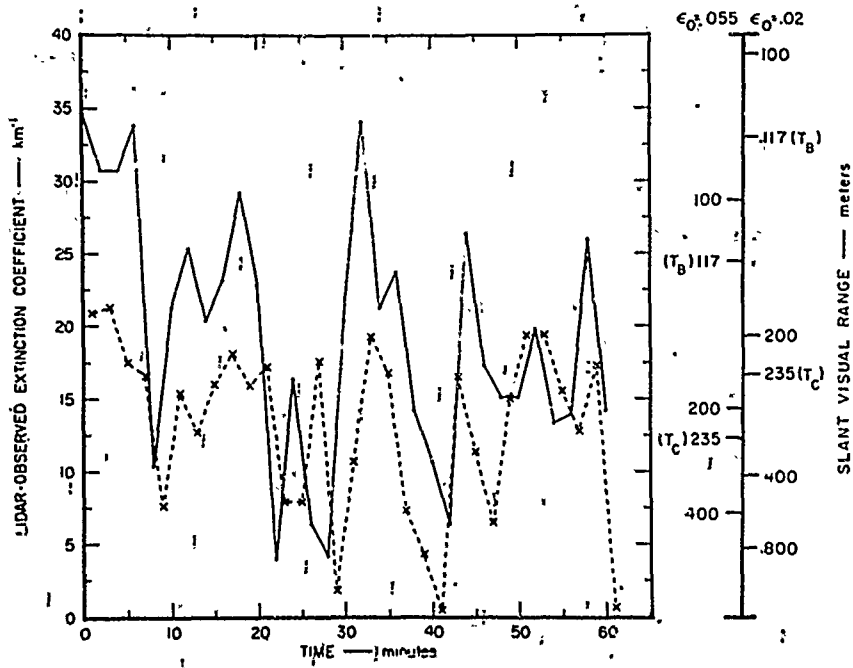

(b) COMPARISON BETWEEN LIDAR-OBSERVED ATMOSPHERIC EXTINCTION COEFFICIENTS DERIVED FROM ELEVATED-TARGET DATA (Dots and Solid Lines) AND FROM SINGLE-ENDED DATA (Crosses and Dashed Lines) DURING CONDITIONS OF LOW CLOUDS AND FOG ON 2 AUGUST 1971, 09:35-10:35 PDT

FIGURE 17

the observed visibility condition of T_B (T_B always visible). The extinction coefficients derived from the single-ended data are lower than those derived from the target data. A possible reason may be that the single-ended data include atmospheric backscatter returns from below the level of the targets, as illustrated in Figure 17(a). Since the density of the fog increased rapidly with height into the stratus clouds, it is not surprising to find the extinction coefficients derived from the elevated targets higher.

To compensate for the effects of a large increase in fog density with height, the single-ended data were reanalyzed by eliminating all data points from the lidar traces up to the distance of target T_A so that the range over which the atmospheric backscatter signal is processed corresponds better to the slant-range distance from T_A to T_B. The recomputed values of atmospheric extinction coefficient are compared with the target-derived coefficients in Figure 18. Truncation of the single-ended data to the distance of target T_A increases the values of the derived extinction coefficient and gives improved agreement with the target-derived values.

Using the data of Figure 18, Figure 19 shows the cumulative percentage frequency with which values of slant visual range were measured by the samples (31 measurements) of target data and single-ended data.

Assuming that these data samples characterize the prevailing fog condition and using the contrast threshold, $\epsilon_o = 0.02$, it is seen that 60 percent of the time the slant visual range predicted on the basis of the lidar data (both target and single-ended data) is less than the 235-m slant-range distance required to see the 200-ft decision-height target, T_C, from the location of the lidar. Furthermore, the data predict that the 100-ft decision-height target, T_B, was visible close to

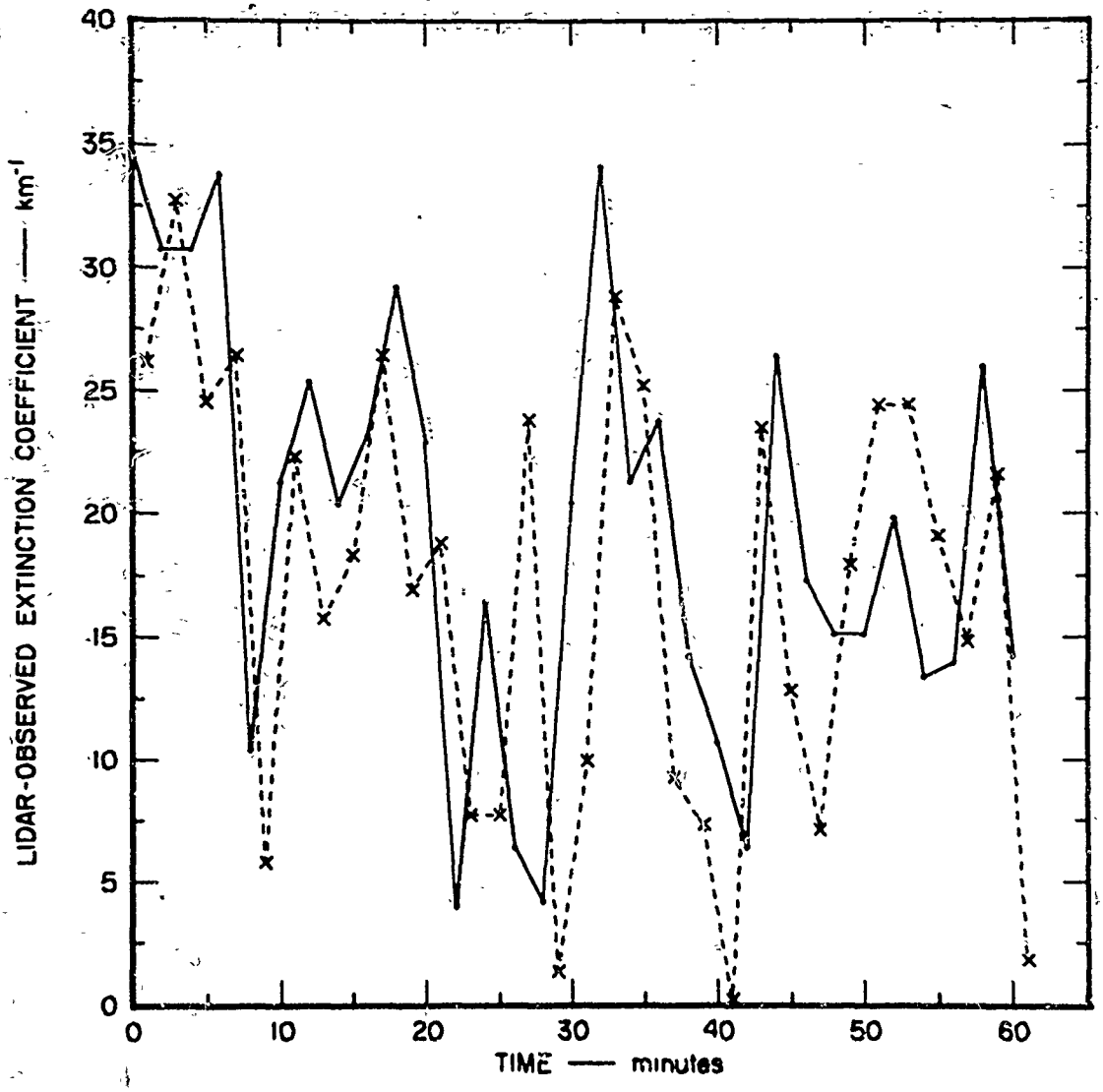

FIGURE 18 IMPROVEMENT IN THE TARGET DATA VERSUS SINGLE-ENDED DATA COMPARISON OF FIGURE 17(b) RESULTING FROM THE TRUNCATION OF THE SINGLE-ENDED LIDAR TRACES TO ACCOUNT FOR LARGE INCREASE OF FOG DENSITY WITH HEIGHT

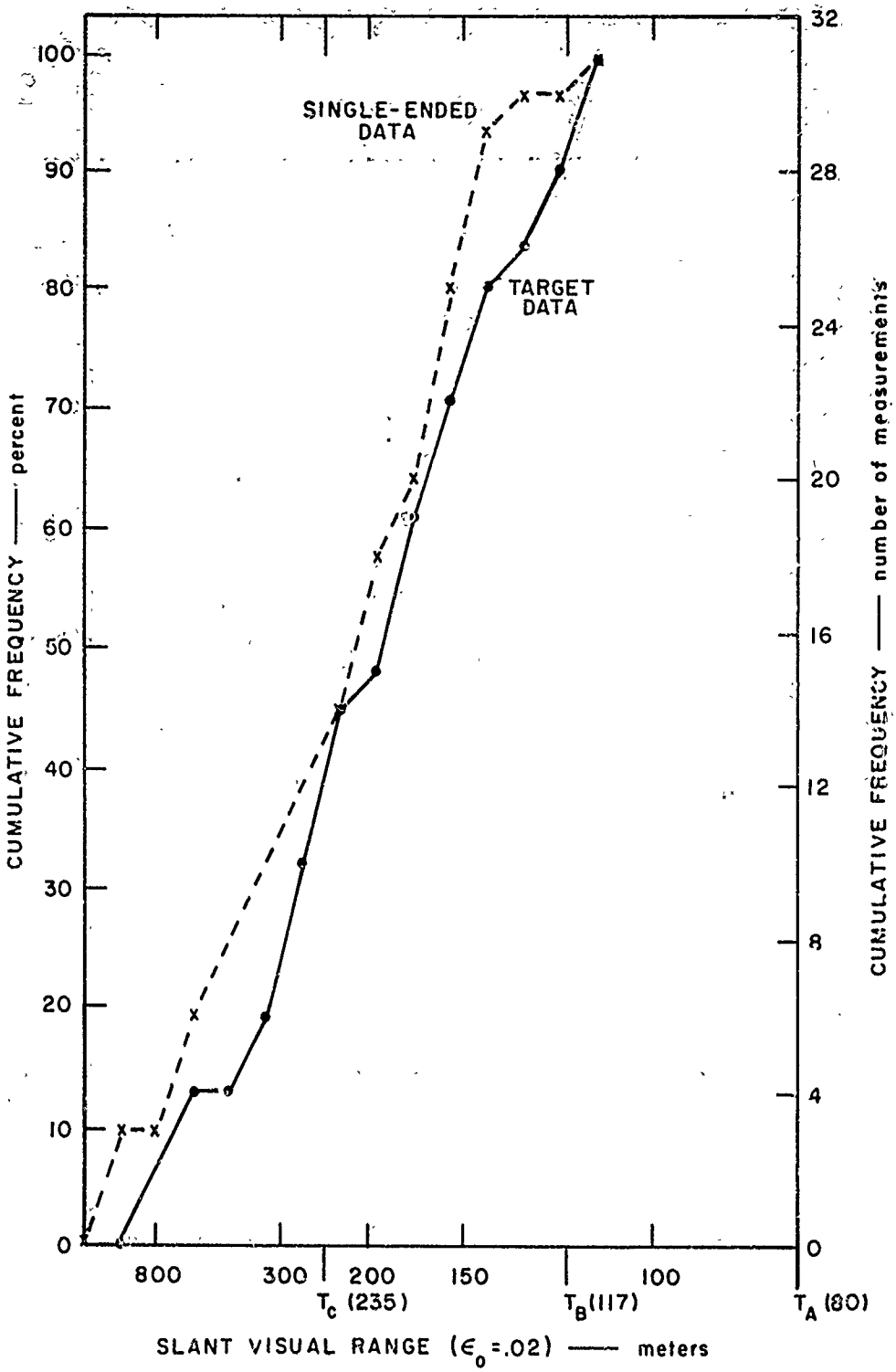

FIGURE 19 CUMULATIVE FREQUENCY OF SLANT VISUAL RANGE PREDICTED BY LIDAR DURING LOW CLOUDS AND FOG ON 2 AUGUST 1971, 09:35-10:35 PDT

100 percent of the time. For $\epsilon_o = 0.055$, these percentages were different and did not as closely relate to what was observed.

During the second period of observation (11:08-11:54 PDT), the 200-ft decision-height target, T_C, was "in and out" of the ragged cloud base, but lidar signals reflected from this target were recorded continuously. Thus, in this case, the target data provide values of the atmospheric extinction coefficient averaged over the slant-path distances from T_A to T_B and from T_B to T_C. These two values were combined into one value averaged over the distance from T_A to T_C (154 m). Figure 20 shows the comparison between the extinction coefficients derived from the (T_A to T_C) target data and from the single-ended data during the period of observation. Before the "slope" method was applied, the single-ended traces of atmospheric backscatter signal versus range were truncated up to the range of target T_A in order to account for the increase of fog density with height. The scale of corresponding values of visual range shows that both the target data and the single-ended data predict clear visibility of T_B and occasional obscuration of T_C. Slant visibilities computed from the lidar-measured extinction coefficients on the basis of a contrast threshold $\epsilon_o = 0.02$ reflect the actual observed visibility conditions better than those computed using the more conservative value $\epsilon_o = 0.055$.

The lidar data of Figure 20 once again show the large temporal fluctuations in slant visibility that are characteristic of the advection-type, coastal fog conditions encountered at Pillar Point. Operationally useful information on slant visibility can only be deduced from time series of individual measurements. Figure 21 shows the cumulative percentage frequency with which values of slant visual range were measured by the target data (22 measurements) and by the single-ended data (24 measurements). Using $\epsilon_o = 0.02$, 45 percent of the target observations but

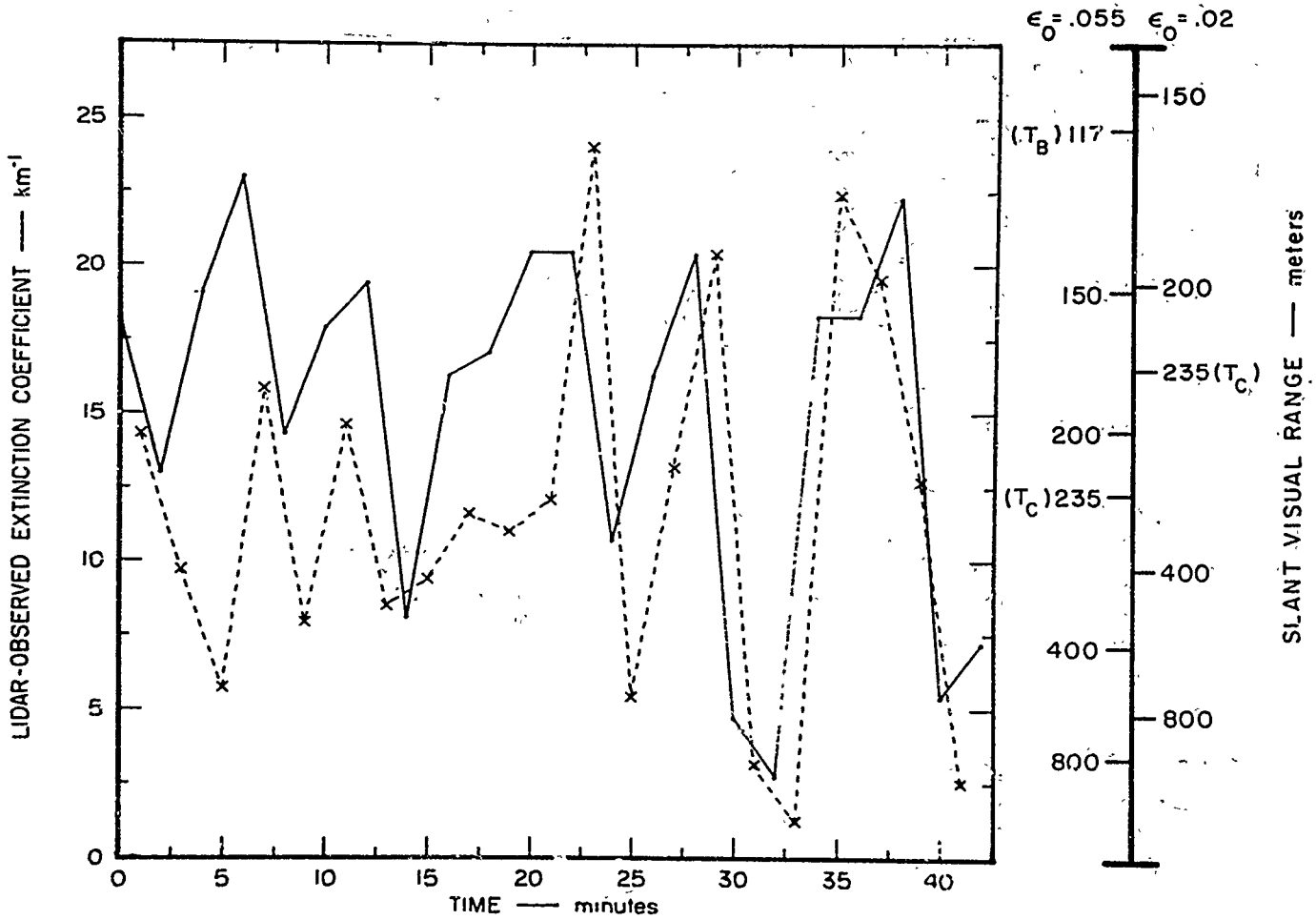

FIGURE 20 TIME SERIES OF SLANT-RANGE ATMOSPHERIC EXTINCTION COEFFICIENT AND CORRESPONDING SLANT VISUAL RANGE OBSERVED BY LIDAR DURING LOW CLOUDS AND FOG ON 2 AUGUST 1971, 10:08-11:54 PDT. Target data--dots and solid lines; single-ended data—crosses and dashed lines.

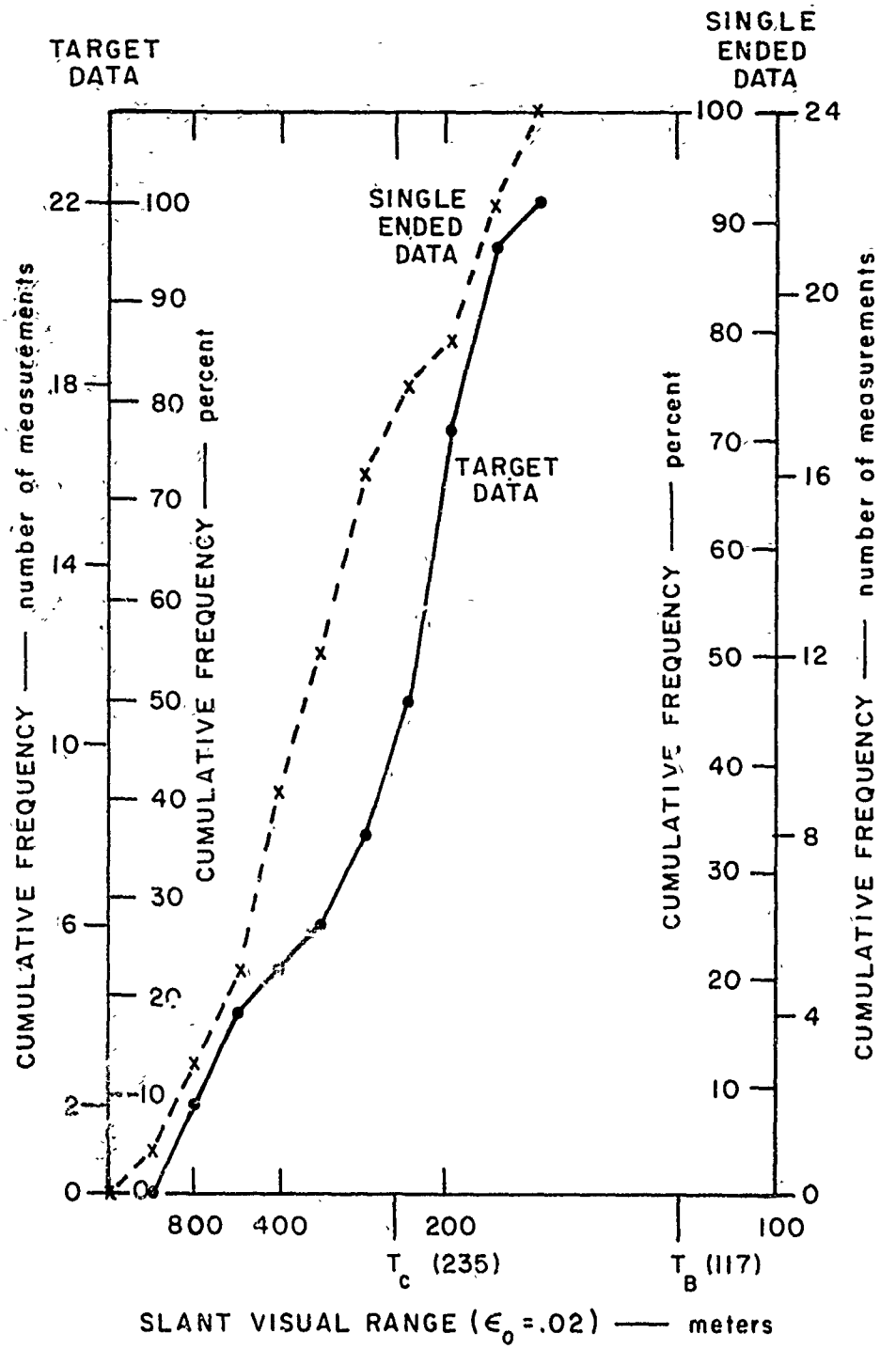

FIGURE 21 CUMULATIVE FREQUENCY OF SLANT VISUAL RANGE OBSERVED BY LIDAR DURING LOW CLOUDS AND FOG ON 2 AUGUST 1971, 10:08-11:54 PDT

75 percent of the single-ended observations predict the 200-ft decision-height target, T_C, to be visible from the location of the lidar (slant visual range of 235 m). Visual observations of T_C suggest that the target data give the more realistic value. The difference in the percentage frequency is caused by the lower values of atmospheric extinction coefficient derived from the single-ended data during the first 20 minutes of observation (see Figure 20). The lidar data recorded during that time showed the occasional presence of a cloud ceiling that was not accounted for in the application of the "slope" method and led to an underestimate of the extinction coefficient.

4. 4 August 1971 (Horizontal Visibility 1000-2000 m)

During a relatively brief period (13:00-15:00 PDT) in the early afternoon of 4 August 1971, low stratus clouds moved in on the field site with the cloud base just below the highest (200-ft decision-height) target T_C. Subsequently, T_C became obscured to the extent that its reflected signal was recorded only intermittently because of rapid lidar-pulse attenuation. Thus, the target data that were collected provide a consistent series of atmospheric extinction coefficients averaged over the slant-path distance T_A to T_B only. Figure 22 shows a sample of computer-processed single-ended data collected between 13:40 PDT and 14:25 PDT. Figure 23 compares the extinction coefficients derived from targets T_A and T_B with those derived from the single-ended data for the same observation period. The extinction coefficients derived from the target data are generally lower than those derived from the single-ended data. This is to be expected since the target data relate only to the lower, "clearer" atmospheric layer. The single-ended data, however, as seen in Figure 22, incorporate the layer above target T_B from which signal returns are obtained over an additional slant-path distance of nearly 80 m. Thus, the higher values of atmospheric extinction obtained from the single-ended

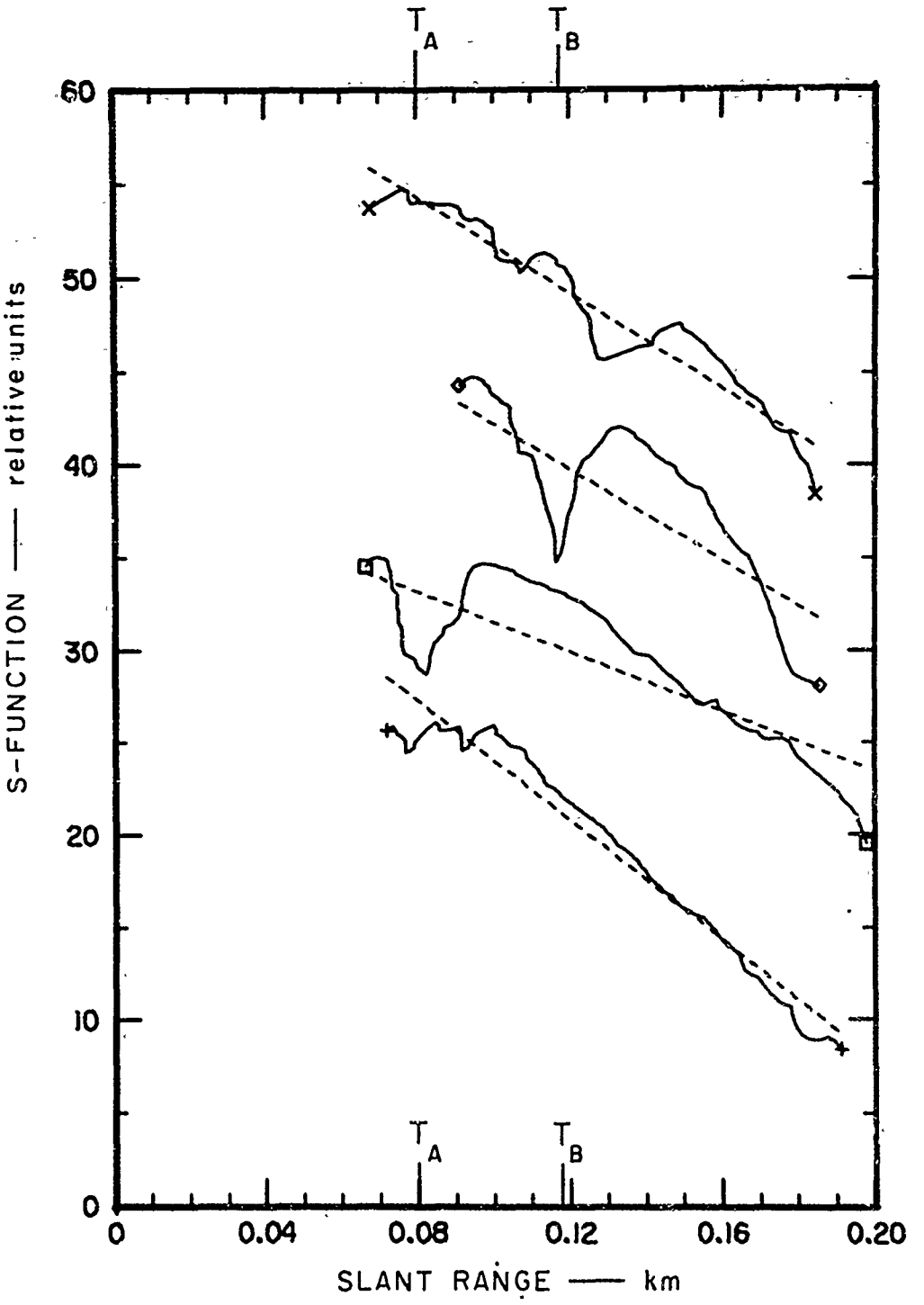

FIGURE 22 SAMPLE OF COMPUTER-PROCESSED SINGLE-ENDED LIDAR DATA OBTAINED ALONG 15° SLANT PATH DURING LOW CLOUDS AND FOG ON 4 AUGUST 1971

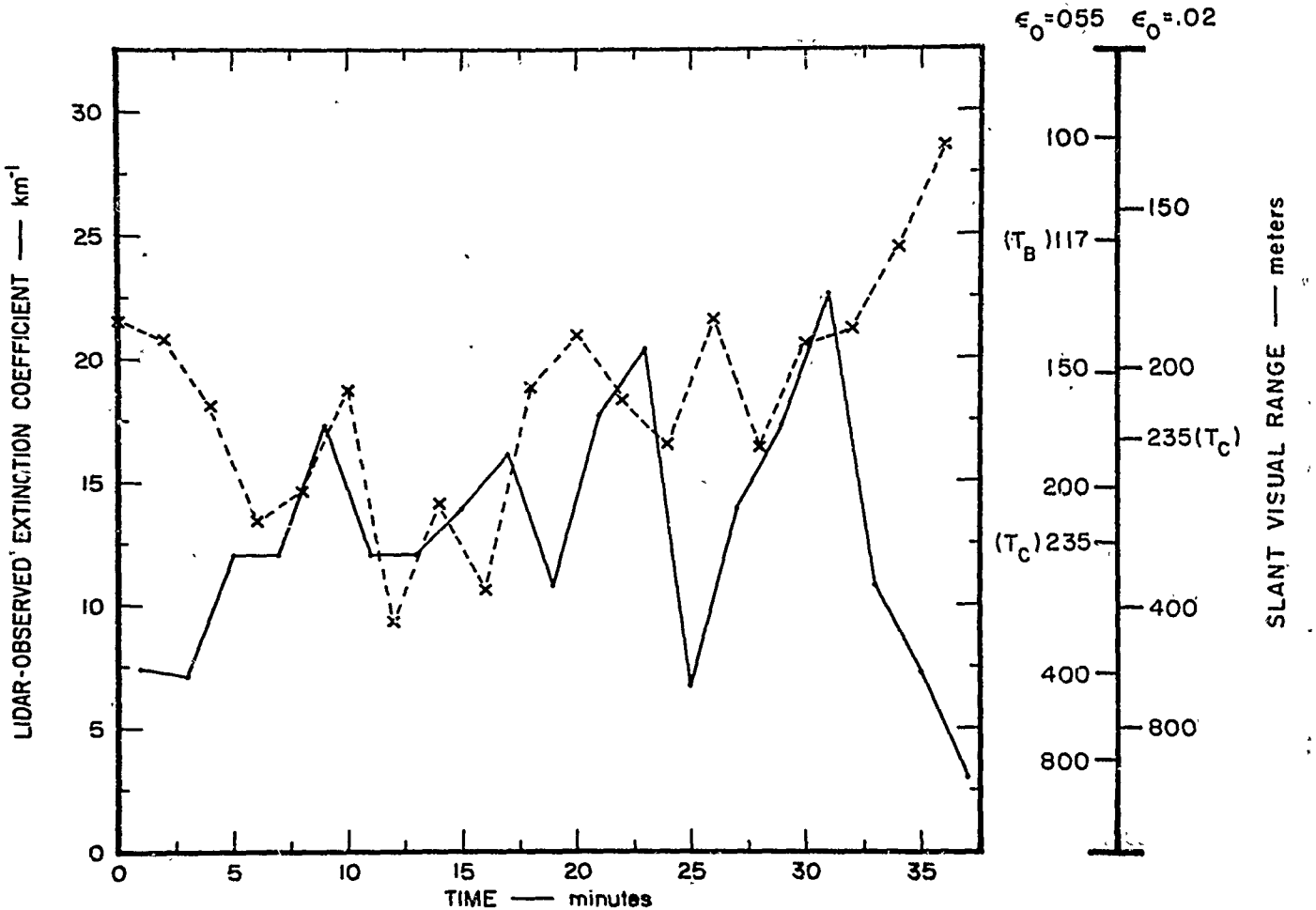

FIGURE 23 COMPARISON BETWEEN SLANT-PATH ATMOSPHERIC EXTINCTION COEFFICIENTS DERIVED FROM TARGETS T_A AND T_B (Dots and Solid Lines) AND FROM SINGLE-ENDED LIDAR DATA (Crosses and Dashed Lines) DURING LOW CLOUDS AND FOG ON 4 AUGUST 1971, 13:40-14:25 PDT

lidar data more accurately represent the atmospheric conditions in which the density of the stratus increases with height into the cloud base. Figure 24 shows the decrease in the extinction coefficients that results when the last 20 data points of each single-ended trace are eliminated from the data analysis--i.e., when the range interval over which the single-ended data of Figure 23 are processed is brought in closer agreement with the distance from T_A to T_B.

Although the total data sample is relatively small (19 single-pulse transmissions), the slant-visibility conditions observed by the lidar data of Figure 23 are summarized in Figure 25. It is seen that the atmospheric extinction coefficients derived from the targets T_A and T_B predict that T_C was visible (slant visual range $\geq$ 235 m) for 75 to 80 percent of the measurements. Actually, T_C was visible less than half of the time. However, since the target data provide extinction coefficients averaged over the slant-path distance from T_A to T_B, they refer to an atmospheric layer in which visibility conditions were obviously better than near the level of T_C. The single-ended traces give a more realistic prediction (T_C only visible for 30 percent of the measurements), because their data apply to a slant-range that extends farther into the low stratus clouds.

5. 5 October 1971 (Horizontal Visibility 70-100 m)

On 1 October 1971, the various problems that arose during the early part of the experimental program due to uncertainties in the characteristics of the logarithmic amplifiers had been resolved to the extent that lidar observations using a dual receiver system could be resumed. The dual receiver system consisted of the upper (low-sensitivity) photomultiplier (pmt 1) connected to logger 1 and the lower (gated) photomultiplier (pmt 2) connected to logger 3.

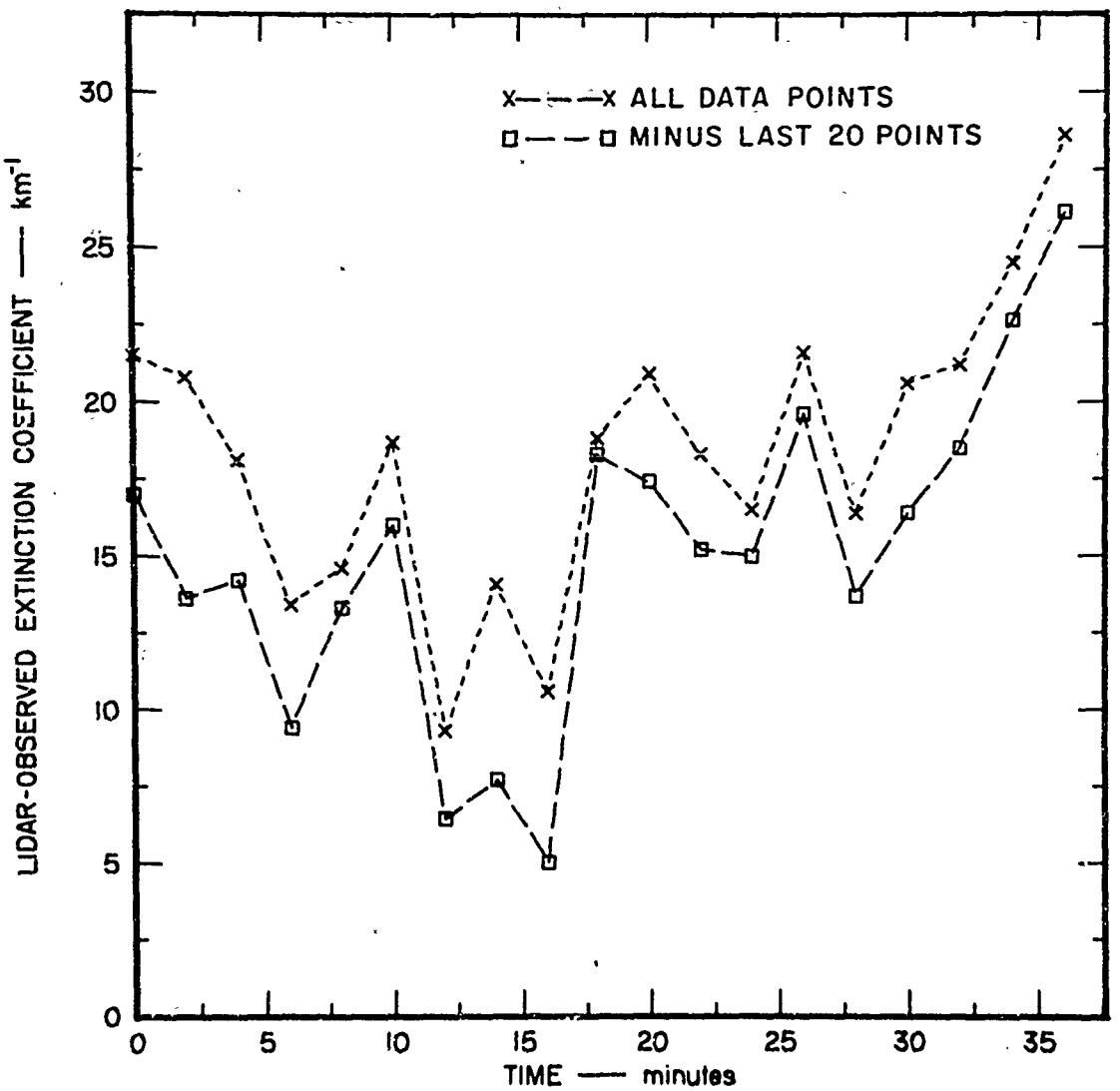

FIGURE 24 DECREASE IN ATMOSPHERIC EXTINCTION COEFFICIENT THAT RESULTS WHEN LAST 20 DATA POINTS OF EACH SINGLE-ENDED TRACE ARE ELIMINATED FROM ANALYSIS (4 AUGUST 1971, 13:40-14:25 PDT)

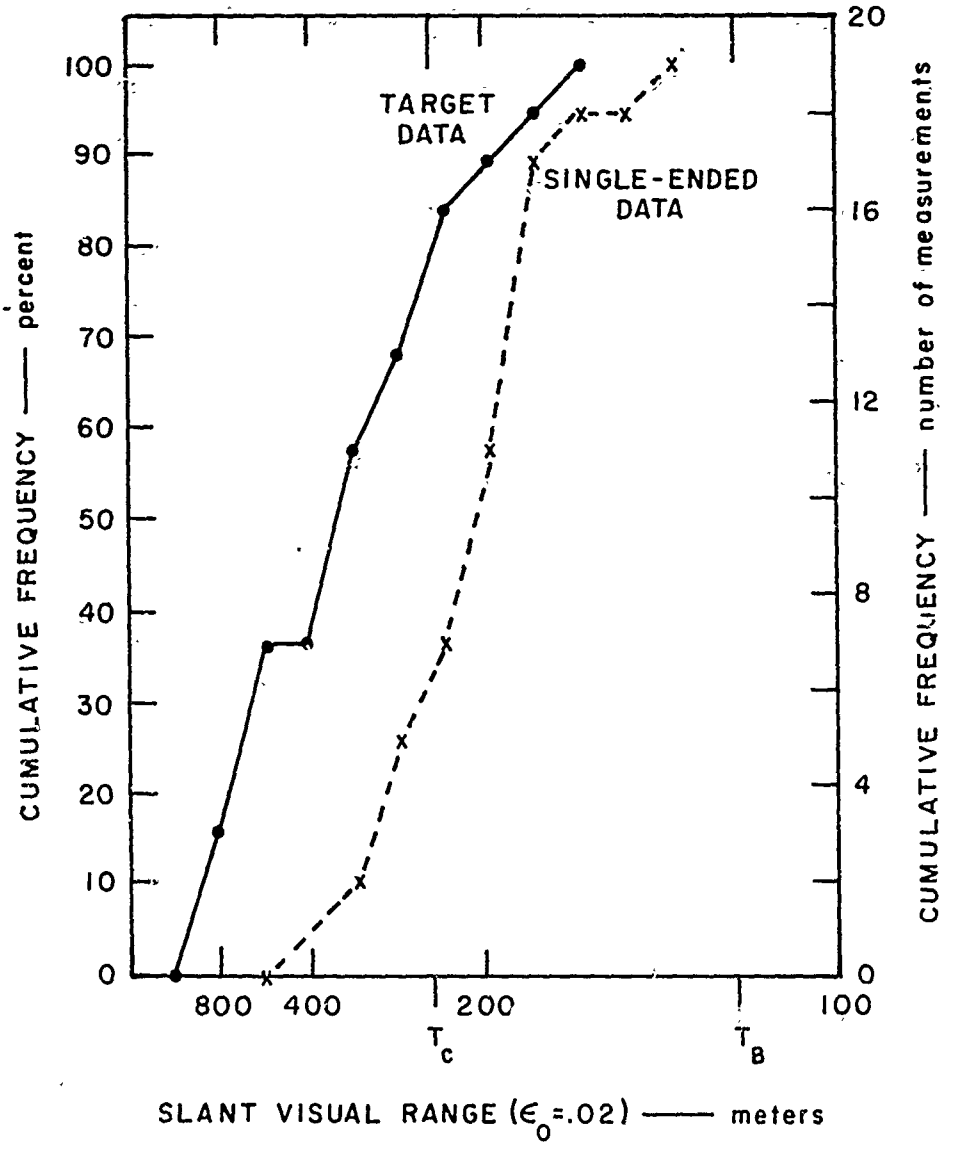

FIGURE 25 CUMULATIVE FREQUENCY OF SLANT VISUAL RANGE MEASURED BY LIDAR DURING LOW CLOUDS AND FOG ON 4 AUGUST 1971, 13:40-14:25 PDT

During the afternoon of 5 October 1971, a dense fog developed at the Pillar Point site, which occasionally reduced horizontal visibility to less than 100 m. The 200-ft decision-height target, T_C, was never visible. The 100-ft decision-height target, T_B, could only occasionally be seen from the location of the lidar, and reflected lidar signals from this target were received only sporadically. T_A remained visible. Thus, atmospheric extinction coefficients from the target data could not be obtained on a continuous basis. Single-ended data of atmospheric backscatter versus range were collected along the 15° slant path adjacent to the elevated targets. Figure 26 shows photographs of oscilloscope traces recorded from the dual-photomultiplier receiver system at two different times. At 15:00 PDT, the recorded data from the low sensitivity photomultiplier (pmt 1) represent what would normally be expected from the coaxial lidar during dense fog: from the minimum useful range (50 m from the location of the lidar), the decrease in atmospheric backscatter signal with range reflects the large atmospheric extinction. At 15:53 PDT, however, when the density of the fog had increased to the extent that target T_A became somewhat obscured, backscatter signals are received from the area between the lidar and the minimum range where the receiver is not supposed to "see" the transmitted lidar beam. Tentatively, these atmospheric backscatter returns are attributed to secondary and higher order (multiple) scatter. It was found that the denser the fog, the more the multiple-scatter effects became noticeable in the recorded data. The "slope" method is applied to the data points beyond the minimum range. To what extent signal returns from multiple scatter are included in our data analysis has not been determined. The "gated" returns from pmt 2/logger 3, shown in Figure 26, give the slope on which the computations of atmospheric extinction coefficient are based. Figure 27 shows values of atmospheric extinction coefficient obtained from the single-ended lidar data by the "slope" method during a 30-minute period. Because of the density of the fog, no consistent series of target data is available for

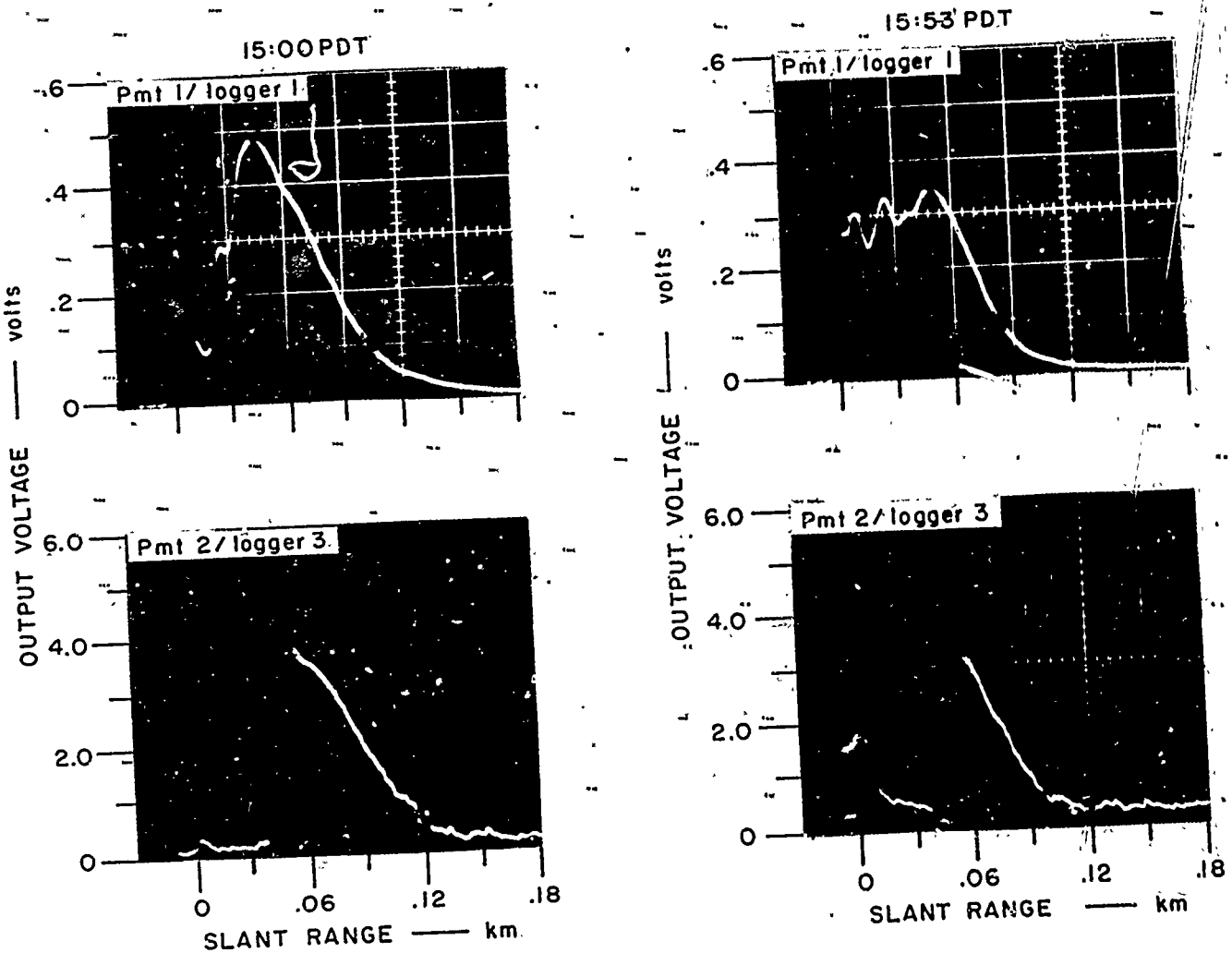

FIGURE 26 OSCILLOSCOPE TRACES OF LIDAR BACKSCATTER SIGNAL VERSUS RANGE RECORDED BY DUAL RECEIVER SYSTEM DURING DENSE FOG AT PILLAR POINT, CALIFORNIA, ON 5 OCTOBER 1971

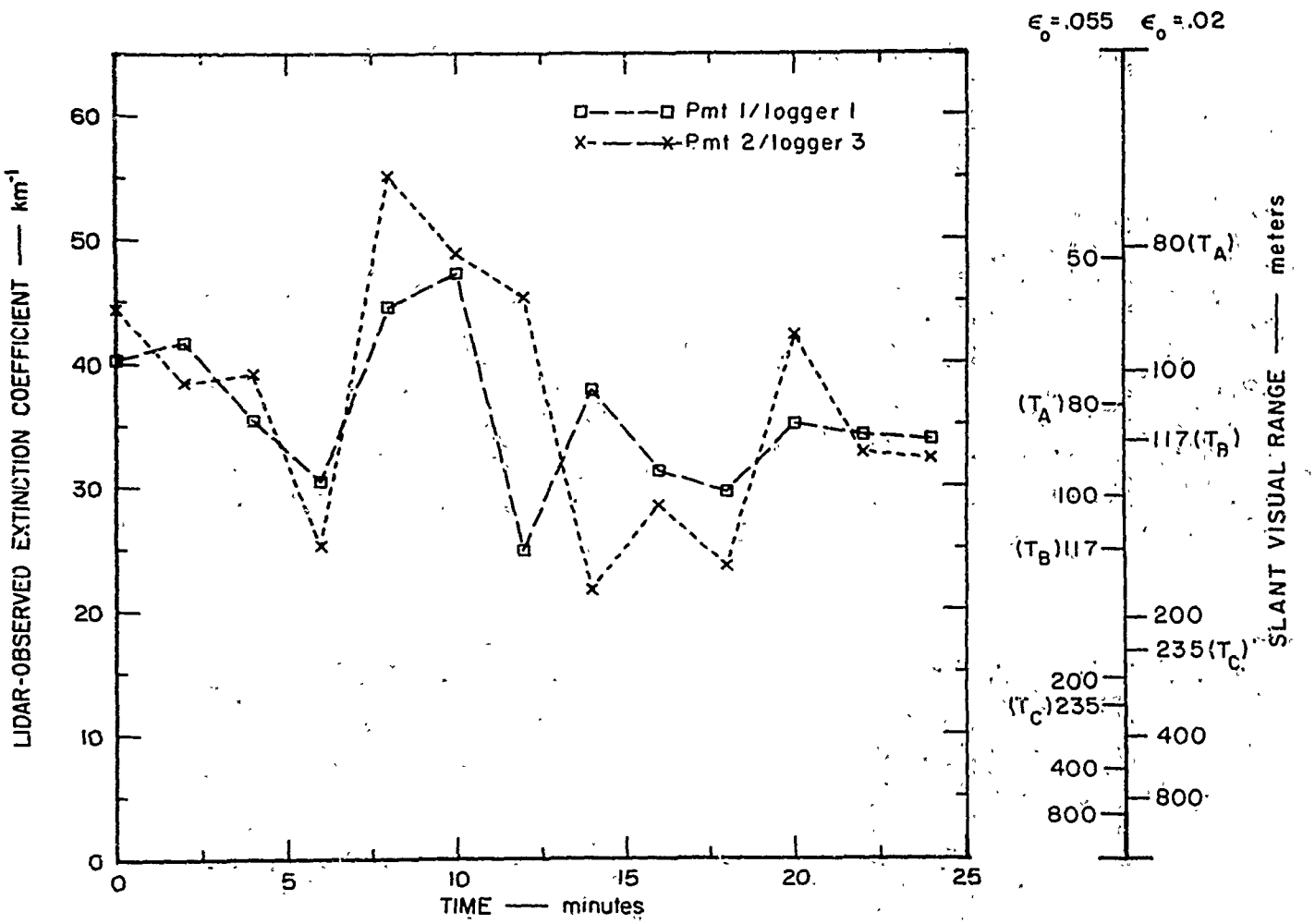

FIGURE 27 TIME SERIES OF SLANT-PATH ATMOSPHERIC EXTINCTION COEFFICIENT AND CORRESPONDING SLANT VISUAL RANGE DERIVED FROM SINGLE-ENDED LIDAR DATA RECORDED SIMULTANEOUSLY BY DUAL RECEIVER SYSTEM ON 5 OCTOBER 1971, 15:45-16:10 PDT

comparison. The single-ended lidar data give a realistic description of the prevailing slant-visibility conditions. Although there is no perfect point-by-point agreement, the variations in the data from pmt 1/logger 1 are quite similar to those from pmt 2/logger 3. The absolute values of extinction coefficient (30 to 50 km^{-1}) are the largest measured during the observational program, which is compatible with the observation that the visibility was the lowest. The difference in absolute values between the data from the two loggers is most likely due to differences in the electrical characteristics of the loggers.

6. 13 October 1971 (Horizontal Visibility 500-800 m)

On 13 October 1971, observations of the elevated targets and of the atmospheric backscatter along the 15° slant path adjacent to the targets were made with the dual receiver system consisting of pmt 1 connected to logger 1 and pmt 2 connected to logger 3. Thus, upon each lidar/pulse transmission, data from two photomultiplier/logarithmic-amplifier components could be recorded simultaneously. Observations were made from 10:22 PDT to 14:07 PDT when dense fog was present. The lowest target, T_A, was clearly visible whereas the 100-ft decision-height target, T_B, was only dimly visible. The 200-ft decision-height target, T_C, was visible only during brief periods from approximately 12:00 to 13:00 PDT and toward the very end of the observation period. The horizontal visibility in the direction of the targets was estimated at 500 m, with a slight improvement to 800 m between 12:00 and 13:00 PDT.

Figure 28 shows a comparison between the atmospheric extinction coefficients derived from the target data recorded simultaneously by pmt 1/logger 1 and pmt 2/logger 3. Measurements of the extinction coefficient were obtained from the reflected signals of targets T_A and T_B and therefore represent values averaged over the slant-path distance from

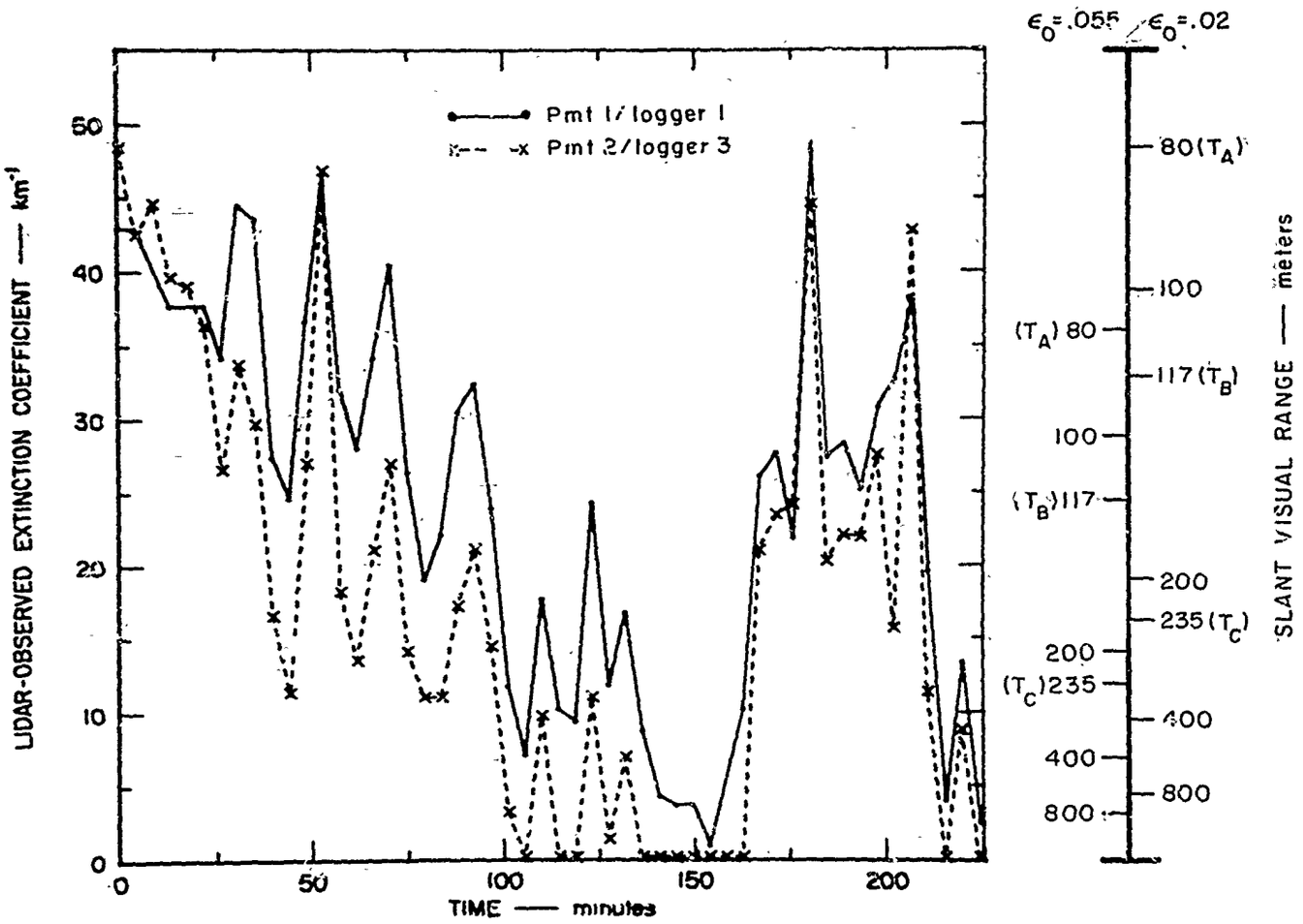

FIGURE 28 TIME SERIES OF SLANT-PATH ATMOSPHERIC EXTINCTION COEFFICIENT AND CORRESPONDING SLANT VISUAL RANGE DERIVED FROM ELEVATED-TARGET DATA RECORDED SIMULTANEOUSLY BY DUAL RECEIVER SYSTEM ON 13 OCTOBER 1971, 10:22-14:07 PDT

T_A to T_B. Reflected lidar signals from T_C were only received intermittently between 12:00 and 13:00 PDT. There is no perfect agreement between the data from the two receiver components. Extinction coefficients deduced from the data of pmt 2/logger 3 are consistently lower and do not represent acceptable values between 12:00 and 13:00 PDT when horizontal visibility improved from 500 to 800 m. It is seen that during this brief period of partial clearing, the extinction coefficients decreased to values representative of visually clear-sky conditions ($\bar{\sigma} \approx 0.1$ km^{-1}). This obvious discrepancy in the data recorded from pmt 2/logger 3 was found to result from insufficient information on the saturation characteristics of the new logarithmic amplifier. The data from pmt 1/logger 1 are reasonable but still show some values of atmospheric extinction near 13:00 PDT that correspond to rather high values of visual range. Slant visual range computed on the basis of $\epsilon_o = 0.02$ gives the best comparison between the target data and visual observations of the elevated targets made at the location of the lidar. For $\epsilon_o = 0.055$, the target data correspond to values of slant visual range that many times are lower than those required to observe target T_B and sometimes lower than those required to observe T_A. This is not in accordance with what actually was observed.

Figure 29 shows the comparison between the atmospheric extinction coefficients derived from single-ended data recorded simultaneously by the two pmt/logger components. There is excellent agreement between the two sets of data, which may indicate that the differences between the target data result from a discrepancy in the signal amplitude-bandwidth characteristic of the new logarithmic amplifier. The atmospheric extinction coefficients obtained from the single-ended data correspond to values of slant visual range that are in complete agreement with what was observed using the threshold constant $\epsilon_o = 0.02$. Table 3 summarizes pertinent information obtained from the data of the two pmt/logger components of the dual receiver system. If it is assumed that the sample

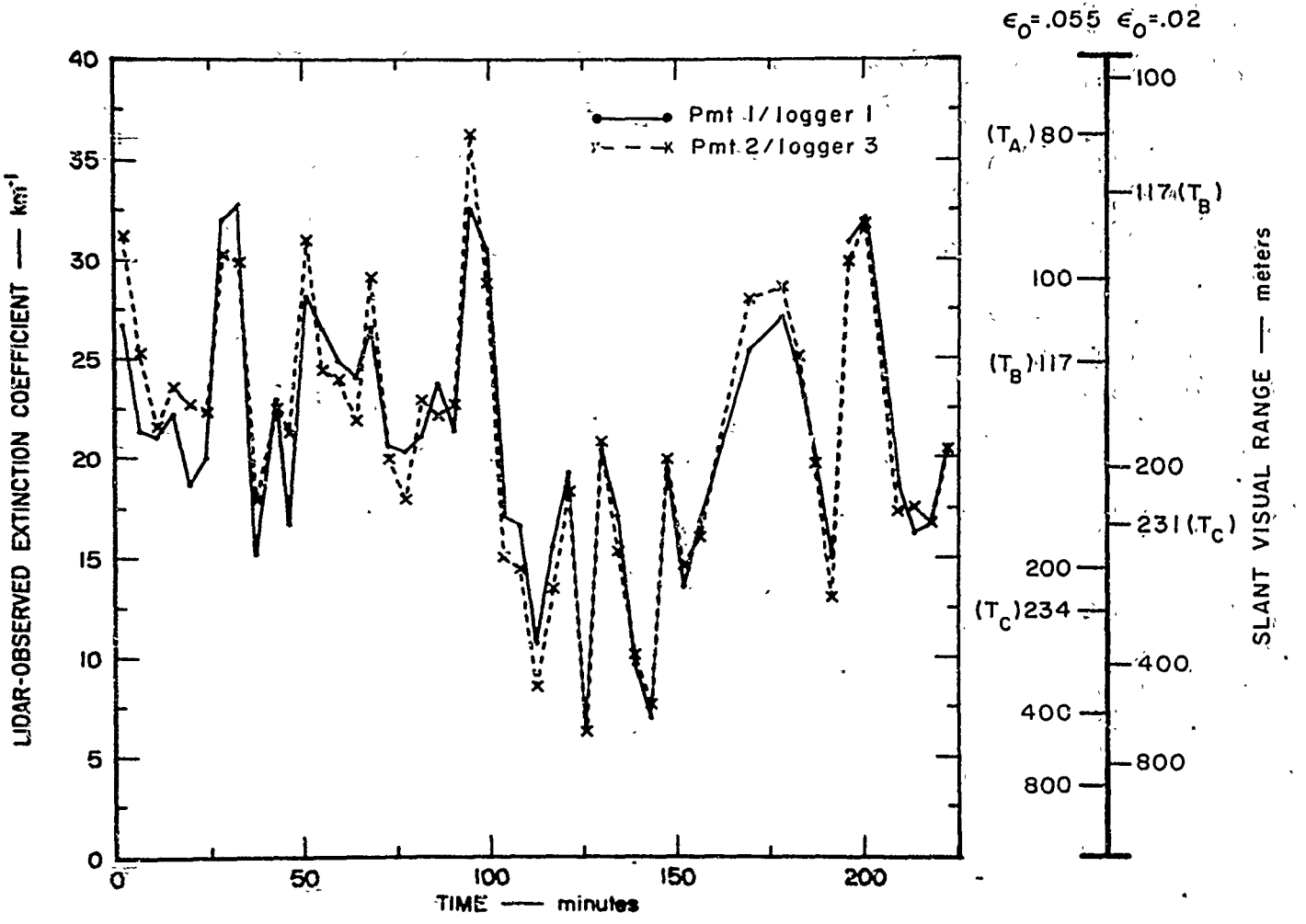

FIGURE 29 COMPARISON BETWEEN SLANT-PATH ATMOSPHERIC EXTINCTION COEFFICIENTS DERIVED FROM SINGLE-ENDED LIDAR DATA RECORDED SIMULTANEOUSLY BY DUAL RECEIVER SYSTEM ON 13 OCTOBER 1971, 10:22-14:07 PDT

Table 3

SUMMARY OF INFORMATION ON SLANT VISIBILITY CONDITIONS OBTAINED FROM LIDAR DATA RECORDED BY THE DUAL RECEIVER SYSTEM OF Mk V LIDAR ON 13 OCTOBER 1971

Receiver Component	Number of Measurements		Ground Visible from 200-ft Height (percent frequency)		Ground Visible from 100-ft Height (percent frequency)	
	Target Data	Single-ended Data	Target Data	Single-ended Data	Target Data	Single-ended Data
pmt 1/logger 1	49	47	30	32	74	97
pmt 2/logger 3	51	47	58	26	90	97

of lidar measurements represents the prevailing fog conditions, the single-ended data predict that the ground would have been visible 97 percent of the time from the 100-ft decision height, but only 26-32 percent of the time from the 200-ft decision height. These percentages are in very good agreement with visual observations of the 100-ft decision height target T_B and the 200-ft decision height target T_C made from the location of the lidar. The results from the target data are not as consistent as those from the single-ended data and reflect the effects of differences in the electrical characteristics of the logarithmic amplifiers.

VI LIDAR MEASUREMENTS OF SLANT VISIBILITY IN THE PRESENCE OF A LOW-CLOUD CEILING

As long as the observed lidar backscatter profiles do not show the sharp increase of received signal versus range associated with a cloud ceiling, the atmospheric extinction coefficients computed by the "slope" method from single-ended lidar backscatter profiles obtained at 15° elevation angle are similar to the slant-path extinction coefficients derived from the target-return signals. The cloud ceiling, however, represents a boundary of extreme inhomogeneity that adversely affects the application of the "slope" method.

Analysis of the lidar data for 23 July 1971 demonstrated that specification of cloud ceiling height enables our computer program to avoid the cloud base and to apply the "slope" method with very good results to the lidar trace above, below, or on either side of the lower cloud boundary.

As an additional task to the contract, a limited sample of lidar data was collected to evaluate to what extent concurrent measurements of cloud ceiling could improve the application of the "slope" method to the slant-range lidar backscatter profiles. Because of the fixed configuration of the lidar for slant-range measurements below 30° elevation, no vertically pointing observations could be made to obtain comparable cloud-ceiling measurements. Instead, a mirror was installed on the nearest tower 75 m from the location of the lidar. This mirror, when inclined at a 45° angle to the lidar's horizontal line of sight, deflects the lidar beam vertically upward for a measurement of cloud base height. While making lidar observations on and off the elevated targets, the setup enables ceiling measurements by simply changing elevation angle within the existing range of operation. Figure 30 shows photographs of the mirror inside its

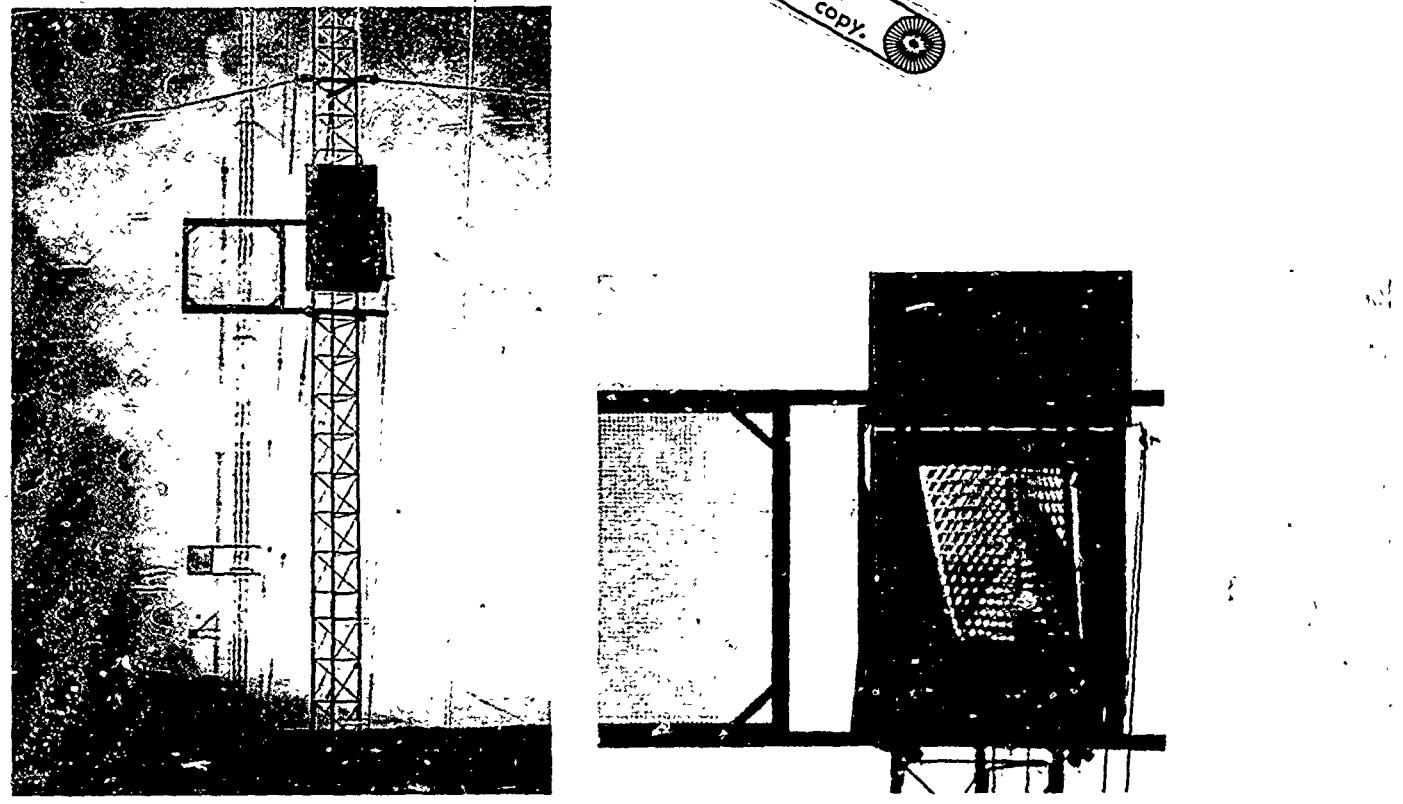

FIGURE 30 PHOTOGRAPHS OF 45° INCLINED MIRROR USED TO DEFLECT LIDAR BEAM FOR MEASUREMENTS OF CLOUD BASE HEIGHT

protective wooden box mounted on the tower nearest to the lidar. An example of a cloud-base measurement obtained by pointing the lidar beam at the inclined mirror is shown in Figure 31.

Measurements of slant visibility and concurrent measurements of cloud-base height were made by alternately aiming the lidar at the mirror (0° elevation angle), at the elevated targets (15° elevation angle), and along the 15° slant path immediately adjacent to the targets. Approximately 5 minutes were needed to make these three separate observations, during which time period significant changes occurred in the highly inhomogeneous fog conditions encountered at the Pillar Point site.

Figure 32 shows the variability in cloud-ceiling height measured with the mirror on a 5-minute time scale during conditions of fog (horizontal visibility 500-800 m) on 13 October 1971. These measurements are related to the lidar-observed extinction coefficients shown in Figures 28 and 29. Also shown are two examples of recorded oscilloscope traces, one with a well-defined cloud ceiling at a height of 39 m above the mirror, the other with the cloud ceiling either at or below the location of the mirror.

It was found that the "mirror" measurements of cloud-base height could not be applied to the analysis of the slant-path, single-ended lidar data because of the rapid time variations in the characteristics of the fog. If cloud-base height has to be considered in the data analysis, measurements must be made simultaneously in time and space with the slant-visibility measurements. Since the effect of a lower cloud boundary on the application of the "slope" method is largest when the increase of atmospheric backscatter with range associated with the cloud base is large--i.e., when the cloud base is clearly defined--the lower cloud boundary can in the most important cases be identified from the slant-path lidar trace itself, and no independent measurement of cloud-base height is needed. Figure 33 shows four consecutive lidar traces of atmospheric backscatter versus range obtained at intervals of 4-5 minutes along the 15° slant path

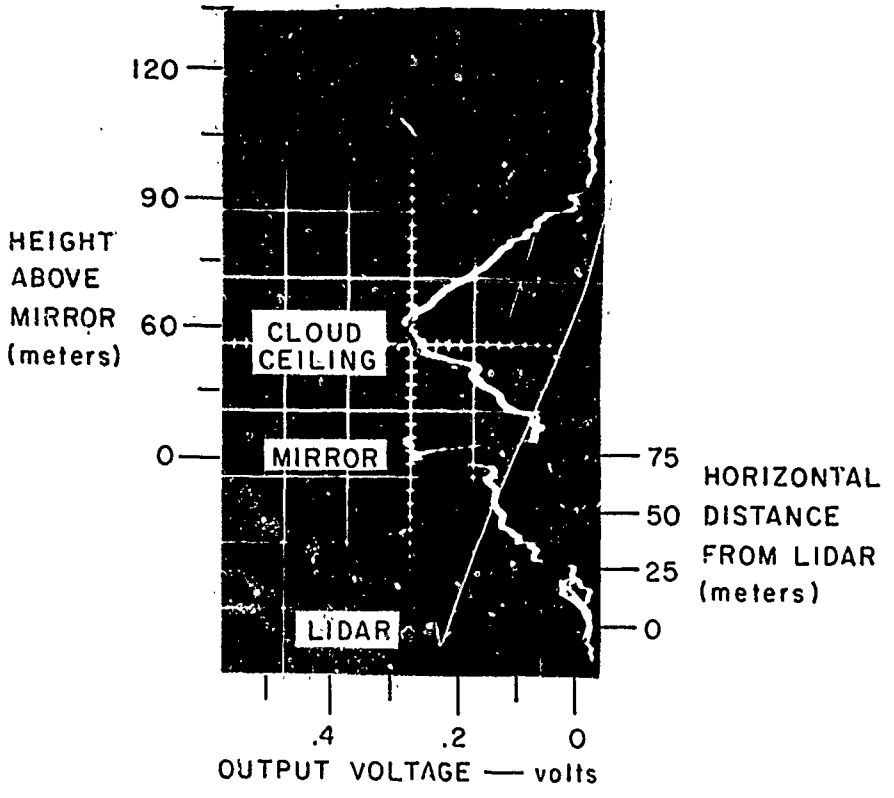

FIGURE 31 OSCILLOSCOPE DISPLAY SHOWING CLOUD CEILING OBTAINED BY POINTING LIDAR BEAM AT 45° INCLINED MIRROR

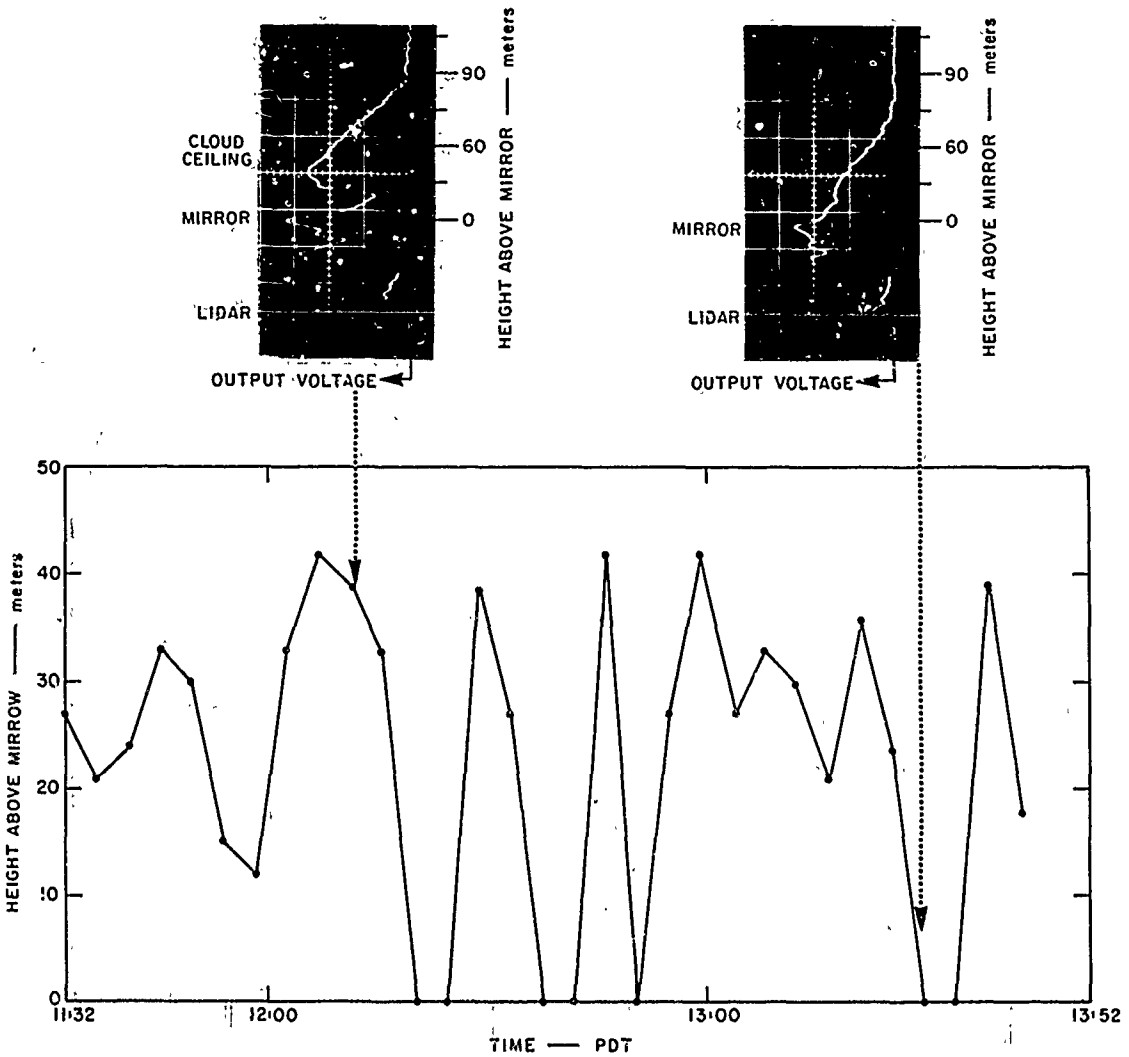

FIGURE 32 TIME SERIES OF LIDAR MEASUREMENTS OF CLOUD BASE HEIGHT USING 45° INCLINED MIRROR (Pillar Point, California, 13 October 1971)

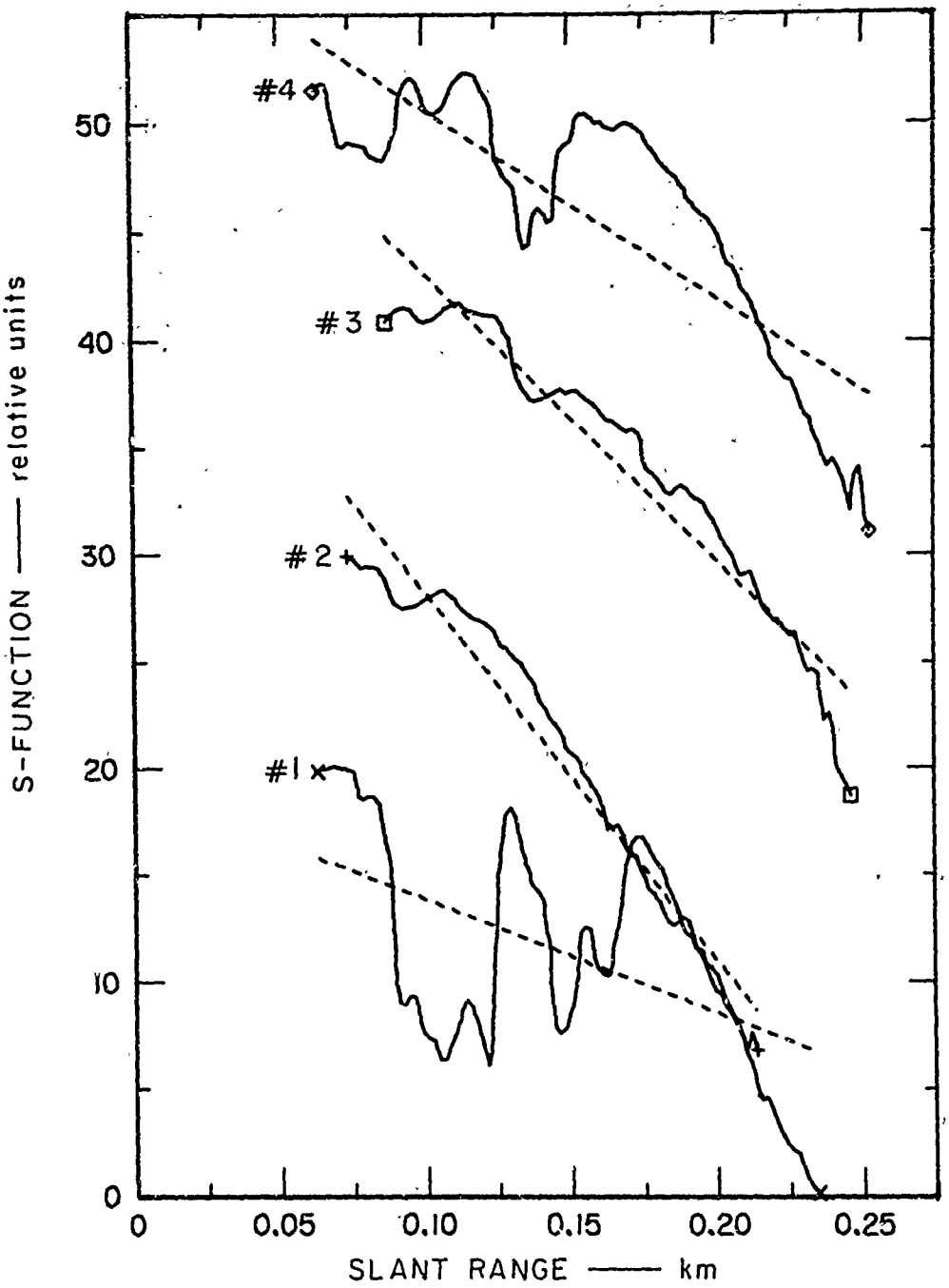

FIGURE 33 LIDAR TRACES OF ATMOSPHERIC BACKSCATTER SIGNAL VERSUS RANGE OBTAINED ALONG 15° SLANT PATH AT 4- TO 5-MINUTE INTERVALS DURING CONDITIONS OF LOW CLOUDS AND FOG ON 13 OCTOBER 1971

adjacent to the elevated targets. The rapid changes in the characteristics of fog are evident. Table 4 lists the improvements in the atmospheric extinction coefficient that are obtained by dividing the traces of Figure 33 into two parts on the basis of a cloud-base height determined from the traces themselves and applying the least-squares procedure separately to each part. Large improvements are evident on Traces 1 and 4. No independent measurements of cloud ceiling are needed to decide how these traces should be broken up. In Traces 2 and 3, the presence of a cloud ceiling is not as apparent, and an independent cloud-ceiling measurement could be helpful. However, in this case, the improvement in the extinction coefficient is relatively small when the cloud-ceiling is accounted for, and therefore the value of a separate cloud-ceiling measurement is not as important. Because of the large spatial and temporal fluctuations in fog density, none of the information from the mirror data recorded during the same period was applicable to any of the traces of Figure 33.

Table 4

ATMOSPHERIC EXTINCTION COEFFICIENTS COMPUTED FROM THE SINGLE-ENDED LIDAR TRACES OF FIGURE 33 BY APPLYING THE "SLOPE" METHOD WITH AND WITHOUT CONSIDERATION OF CLOUD CEILING

Trace	Range of Estimated Cloud Ceiling (km)	Atmospheric Extinction Coefficient (km^{-1})	
		Without Cloud Ceiling	With Cloud Ceiling
No. 1	0.175	6.1	15.9
No. 2	0.110	19.9	20.8
No. 3	0.149	15.4	14.8
No. 4	0.155	10.0	14.2

REFERENCES

Brown, Richard T., Jr., "Backscatter Signature Studies for Horizontal and Slant Range Visibility," Final Report, Contract FA65WA-1315, Federal Aviation Agency (May 1967).

Collis, Ronald T. H., William Viezee, Edward E. Uthe, and John Oblanas, "Visibility Measurement for Aircraft Landing Operations," Final Report, Contract No. F 19628-70-C-0083, Air Force Cambridge Research Laboratories (September 1970).

Hering, Wayne S., H. Stuart Muench, and H. Albert Brown, "Field Test of a Forward Scatter Visibility Meter," Environmental Research Papers, No. 356, Air Force Cambridge Research Laboratories (May 1971).

Viezee, William, Edward E. Uthe, and Ronald T. H. Collis, "Lidar Observations of Airfield Approach Conditions: An Exploratory Study," JAM, Vol. 8, No. 2 (April 1969).